Regulation of amyloid processing in neurons by astrocyte-derived cholesterol

Hao Wang[1,2,3,6], Joshua A. Kulas[4,5,6], Heather A. Ferris[4,5*], Scott B. Hansen[1,2*]

[1]Department of Molecular Medicine, [2]Department of Neuroscience, [3]Skaggs Graduate School of Chemical and Biological Sciences, The Scripps Research Institute, Jupiter, FL 33458, USA
[4]Division of Endocrinology and Metabolism, [5]Department of Neuroscience, University of Virginia, Charlottesville, VA 22908, USA; [6]these authors contributed equally

*Correspondence: shansen@scripps.edu, hf4f@virginia.edu

ABSTRACT

Alzheimer's Disease (AD), a common and burdensome neurodegenerative disorder, is characterized by the presence of β-Amyloid (Aβ) plaques, inflammation, and loss of cognitive function. A cholesterol-dependent process sorts Aβ-producing enzymes into nanoscale lipid compartments (also called lipid rafts). Genetic variation in a cholesterol transport protein, apolipoprotein E (apoE), is the most common genetic marker for sporadic AD. Evidence suggests apoE links to Aβ production through lipid rafts, but so far there has been little scientific validation of this link in vivo. Here we use super-resolution imaging to show apoE utilizes astrocyte-derived cholesterol to specifically traffic amyloid precursor protein (APP) into lipid rafts where it interacts with β- and γ-secretases to generate Aβ-peptide. We find that targeted deletion of astrocyte cholesterol synthesis robustly reduces amyloid burden in a mouse model of AD. Treatment with cholesterol-free apoE or knockdown of cholesterol synthesis in astrocytes decreases cholesterol levels in cultured neurons and causes APP to traffic out of lipid rafts where it interacts with α-secretase and gives rise to soluble APPα (sAPPα), a neuronal protective product of APP. Changes in cellular cholesterol have no effect on α-, β-, and γ-secretase trafficking, suggesting the ratio of Aβ to sAPPα is regulated by the trafficking of the substrate, not the enzymes. Treatment of astrocytes with inflammatory cytokines IL-1β, IL-6 and TNF-α upregulates the synthesis of cholesterol in the astrocytes. We conclude that cholesterol is a signaling molecule kept low in neurons to inhibit raft function, decrease Aβ formation, and enable astrocyte regulation of APP by cholesterol control of substrate presentation.

Highlights:

ApoE regulates amyloid precursor protein localization to rafts and its exposure to α- vs. β-secretase.
α-, β-, and γ-Secretases are activated by substrate presentation.
ApoE specifically transports astrocyte cholesterol to neurons.
Astrocyte cholesterol synthesis disruption prevents Alzheimer's-associated amyloid pathology in mice.

INTRODUCTION

Alzheimer's disease (AD), the most prevalent neurodegenerative disorder, is characterized by progressive loss of cognitive function and the accumulation of amyloid β (Aβ) peptide[1]. The loss of cognitive function is thought to involve aggregates of Aβ peptide, a small hydrophobic protein excised from the transmembrane domain of amyloid precursor protein (APP) by proteases known as gamma- (γ-) and beta- (β-) secretases (Figure S1a). In high concentration Aβ peptide is toxic and aggregates of Aβ form plaques. In healthy individuals, Aβ peptide cycles daily with sleep[2,3] and appears to have antimicrobial activity[4]. A third enzyme, alpha- (α-) secretase generates a soluble APP fragment (sAPPα) which, in healthy individuals, helps set neuronal excitability[5]. α-secretase-mediated APP cleavage and prevents Aβ production, and thus is protective and considered the non-amyloidogenic pathway, whereas sequential β- and γ-secretase-mediated APP cleavage is called the amyloidogenic pathway[6]. Both pathways are finely regulated by cholesterol[7](Figure S1b).

In cellular membranes, cholesterol regulates the formation of lipid domains (also known as lipid rafts) and the affinity of proteins to lipid rafts[8] including β-secretase and γ-secretase[9–11]. α-Secretase does not reside in lipid rafts, rather α-secretase is thought to reside in a region made up of disordered polyunsaturated lipids, separated

from rafts[12]. The location of APP is less clear, in detergent resistant membranes (DRMs) studies it primarily associates with lipid from the disordered region, although not exclusively[9,11,13,14]. Endocytosis is thought to bring APP in proximity to β-secretase and γ-secretase and this correlates with Aβ production. Cross linking of APP with β-secretase on the plasma membrane also increases Aβ production, leading to a hypothesis that raft localization contributes to APP processing[12,15] (Figure S1a). Testing this hypothesis *in vivo* has been hampered by the small size of lipid rafts (often <100 nm), which is below the resolution of light microscopy.

Recently super resolution imaging has emerged as a complimentary technique to DRM's, with the potential to interrogate raft affinity more directly in a native cellular environment[16]. We recently employed super resolution imaging to directly demonstrate a process called substrate presentation[17]. In substrate presentation, increases of cholesterol causes lipid rafts to sequester the enzyme away from its substrate, removal of cholesterol then releases and activates the enzyme by giving it access to its substrate (Figure S1c)[8,17]. A similar mechanism has been proposed to regulate the exposure of APP to its cutting enzymes[12,15,18–20].

Neurons are believed to be the major source of Aβ in normal and AD brains[21,22]. In the adult brain, the ability of neurons to produce cholesterol is impaired during development[23]. Instead, astrocytes make cholesterol and transport it to neurons with apolipoprotein E (apoE)[24–26]. Interestingly, apoE, specifically the e4 subtype (apoE4), is the strongest genetic risk factor associated with sporadic AD[27,28]. This led to the theory that apoE may be controlling Aβ formation through regulation of lipid raft function[12,15,18]. Here we show that astrocyte-derived cholesterol controls Aβ formation *in vivo* and links inflammatory cytokines, apoE, Aβ, and plaque formation to a single molecular pathway.

RESULTS

Characterization of lipid raft prevalence in *brain tissue*.

To establish a role for Aβ regulation by lipid rafts *in vivo*, we first labeled and imaged monosialotetrahexosylganglioside1 (GM1) lipids in mouse brain slices. GM1 lipids reside in cholesterol dependent lipid rafts and bind cholera toxin B (CTxB) with high affinity[29,30]. These lipid rafts or GM1 domains are separate from phosphatidylinositol 4,5 bisphosphate (PIP_2) domains, which are polyunsaturated and cholesterol independent[17,31,32]. We labeled GM1 domains (i.e. lipid rafts) from cortical slices with Alexa Fluor 647 conjugated fluorescent CTxB, and imaged with confocal and super-resolution direct stochastical optical reconstruction microscopy (dSTORM)[33–36]. dSTORM is capable of visualizing nanoscale arrangements (i.e. sub-100 nm diameter lipid domain structures[37]) in intact cellular membranes.

CTxB appeared to label most cell types in cortical brain slices (Figure 1a, green shading). By zooming in on neurons, labeled with antibody against neurofilament medium chain (NFM), a neuronal specific protein, CTxB can be seen outlining the plasma membrane (outside of the cell) as opposed to NFM which labels throughout the cells (Figure 1a right panels).

We used dSTORM (an ~10-fold increase in resolution compared to confocal) to characterize the relative size and number of GM1-domains in mammalian brain tissue (Figure 1c). Cortical tissue from mouse averaged ~141 nm in apparent diameter, a diameter slightly smaller than the apparent size in primary neurons (~150 nm diameter) (Figure 1c). N2a cells exhibited the smallest rafts by far, on average only 100 nm in apparent diameter. All of the mammalian cells had domains larger than what we saw in intact fly brain which had an apparent diameter of ~90 nm[38]. Lipid rafts were also measured in neurons with the SREBP2 gene ablated in cocultured astrocytes. SREBP2 is an essential regulator of cholesterol synthesis enzymes[39] and was specifically knocked out in astrocytes using an ALDH1L1 promoter driven Cre recombinase[40]. The raft size of primary neurons cultured with SREBP2-/- astrocytes was significantly reduced (130 nm), suggesting that astrocyte derived cholesterol contributes to cholesterol content of neuronal membranes.

Since GM1 domains are cholesterol dependent, to confirm that apoE is regulating GM1 domain formation *in vivo*, we added apoE to primary

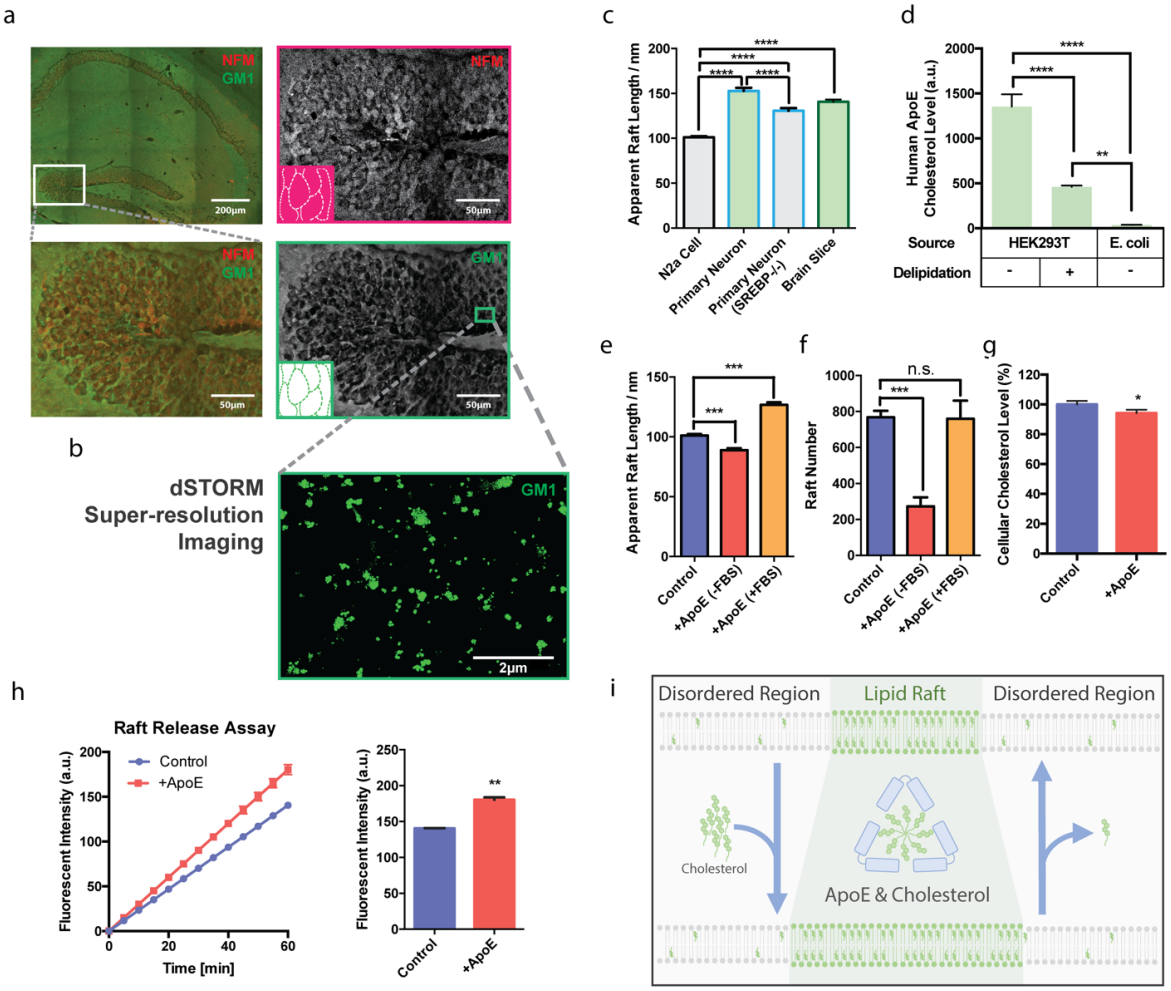

Figure 1. ApoE inserts and sequesters cholesterol to modulate lipid raft characteristics. (a) Confocal imaging on mouse brain showing GM1 lipids in plasma membrane of neurons. Neurons are labelled with neurofilament medium chains (NFM) antibody (red) and GM1 lipids are labelled with fluorophore-conjugated cholera-toxin B subunit (CTxB, green). Representative images showing NFM filled the cell bodies of hippocampal neurons while GM1 lipids are in the plasma membrane. (b) dSTORM super resolution imaging on brain slices showing lipid raft nano-structure in cell membrane. Scale bar is 2 μm. (c) Comparison of apparent raft length in N2a cells, primary neurons cultured with astrocytes with and without cholesterol synthesis and brain slices. Primary neurons and brain slices have relatively larger rafts compared with N2a cells. Neurons cultured with cholesterol depleted astrocytes have relatively smaller rafts compared with neurons cultured with healthy astrocytes. (d) Level of cholesterol carried by purified apoE protein measured by a fluorescent based cholesterol assay. Human apoE expressed by mammalian cells HEK293T carries high level of cholesterol. After delipidation, a large amount of cholesterol is removed. Human apoE expressed by *E. coli* (used for imaging and biochemical studies in this paper) carries little cholesterol. (e) Quantitation of raft lengths indicates changes in raft structure after apoE treatment. (f) Quantitation of GM1 clusters shows apoE decreased the number of rafts under low cholesterol conditions, while apoE treatment with high environmental cholesterol didn't affect raft number. Data are expressed as mean ± s.e.m., *P<0.05, **P<0.01, ***P<0.001, ****P<0.0001, one-way ANOVA. (g) Exposure of neuroblastoma 2a (N2a) cells to apoE removes cholesterol from cellular membrane as measured by a fluorescent based cholesterol assay. (h) Raft release assay showing treatment of N2a cells with apoE causes a palmitoyl reporter enzyme to exit the raft and produce fluorescent product (see methods). Data are expressed as mean ± s.e.m.. *P<0.05, **P<0.01, two-sided Student's t-test. (i) Under low cholesterol conditions, apoE (blue cartoon) extracts cholesterol (green cartoon) from cell membrane, thereby disrupting lipid raft integrity. When presented cholesterol, apoE transports cholesterol into the membrane, forming lipid-ordered domains and stabilizing lipid rafts.

neurons and N2a cells. The apoE (human subtype 3) derived from *E. coli* was devoid of cholesterol, as prokaryotes do not make cholesterol (Figure 1d). To provide apoE a source of cholesterol we added 10% fetal bovine serum (FBS), a common source of mammalian lipids including cholesterol (~310 µg/mL in FBS) containing lipoproteins. ApoE can both load and unload cholesterol from cells, including neurons, dependent on a source of cholesterol[41–43]. Cells were treated with 4 µg/mL of apoE, a physiologically relevant concentration seen in cerebral spinal fluid[44].

Loading cells with cholesterol (apoE +FBS) caused an increase in the apparent raft diameter from 100 nm to 130 nm in N2a cells (Figure 1e). When cholesterol was unloaded, i.e., effluxed (ApoE -FBS), the apparent size and number of GM1 domains decreased (Figure 1e-f). To confirm this result, we compared apoE treatment to treatment with methyl β-cyclodextrin (MβCD), a non-native chemical binder that also extracts cholesterol from the plasma membrane and disrupts raft function[45]. MβCD caused a similar decrease as seen for cells with cholesterol effluxed (Figure S2a). Binning rafts by large > 500 nm and small < 150 nm showed a clear shift toward smaller domains with apoE in low cholesterol and a clear shift to large domains with apoE in high cholesterol (Figure S5b-d).

To investigate the lipids effluxed from the plasma membrane by apoE, we expressed a FLAG tagged apoE in mammalian HEK293 cells, delipidated the protein, exposed it to N2a cultures, isolated the exposed protein, and then quantitated the lipids. ApoE appeared to bind primarily cholesterol (Figure S6a-b). Some saturated lipids were also extracted from the membrane by apoE, suggesting apoE may not only disrupt rafts through cholesterol depletion but may also induce raft removal through extracting saturated lipids (Figure S6c). However, the results are complicated by the fact that we were unable to completely delipidate the apoE prior to exposing it to cell membranes (Figure 1d).

We have also investigated apoE's effect in modulating membrane cholesterol level and lipid raft integrity using a cholesterol assay and a phospholipase D (PLD)-based raft release assay, respectively. We showed N2a's total cellular cholesterol level decreased after 1 h incubation with apoE (-FBS) (Figure 1g). PLD is activated by cholesterol depletion from GM1 domains[17]. ApoE disrupted GM1 domain function and increased PLD activity (Figure 1h). These results suggest a functional role of apoE in extracting cellular cholesterol and disrupting lipid rafts.

Super resolution imaging of amyloid processing proteins in lipid rafts.

Next we sought to characterize the effect of cholesterol loading on GM1 domain function, i.e. the ability of GM1 domains to traffic APP towards or away from its hydrolyzing secretases. Trafficking of APP by apoE in and out of GM1 domains is separate from its ability to regulate the total number of rafts. Based on previous experiments with MβCD[12,15,18] we expected cholesterol efflux by apoE should decrease Aβ formation, but this needed to be established experimentally in intact membranes.

To establish the trafficking of APP to each of its processing enzymes, α, β, and γ, -secretases, in the plasma membranes of intact cells, we imaged neuroblastoma 2a (N2a) cells with dSTORM. APP was previously found in both raft and non-raft like fractions of DRMs[9,11,13,14]. Detergent resistant membranes are similar to GM1 lipid rafts, but not identical. Imaging APP is particularly important since the amount of raft-like association in DRM's could easily be affected by detergent concentration used in their preparation. To image APP directly by dSTORM we labeled GM1 domains with fluorescent CTxB and the amyloid proteins (APP, α, β, and γ, -secretases) with Cy3b labeled fluorescent antibodies and determined raft localization by pair correlation using DBSCAN of two color dSTORM images (Figure 2a).

Figure 2b-e (blue bars) shows APP, β-secretase, and γ-secretase are associated with GM1 raft lipids (i.e. they exhibit strong pair correlation with CTxB labeled GM1 lipids at short distances (0-5nm)). In contrast, α-secretase is not associated with GM1 domains (i.e. lacks pair correlation with CTxB) (Figure 2f, blue bar). The pair correlation (a unitless number) ranged from 10-15 for APP, β-secretase, and γ-secretase while the pair correlation for α-secretase was <3, a value typical

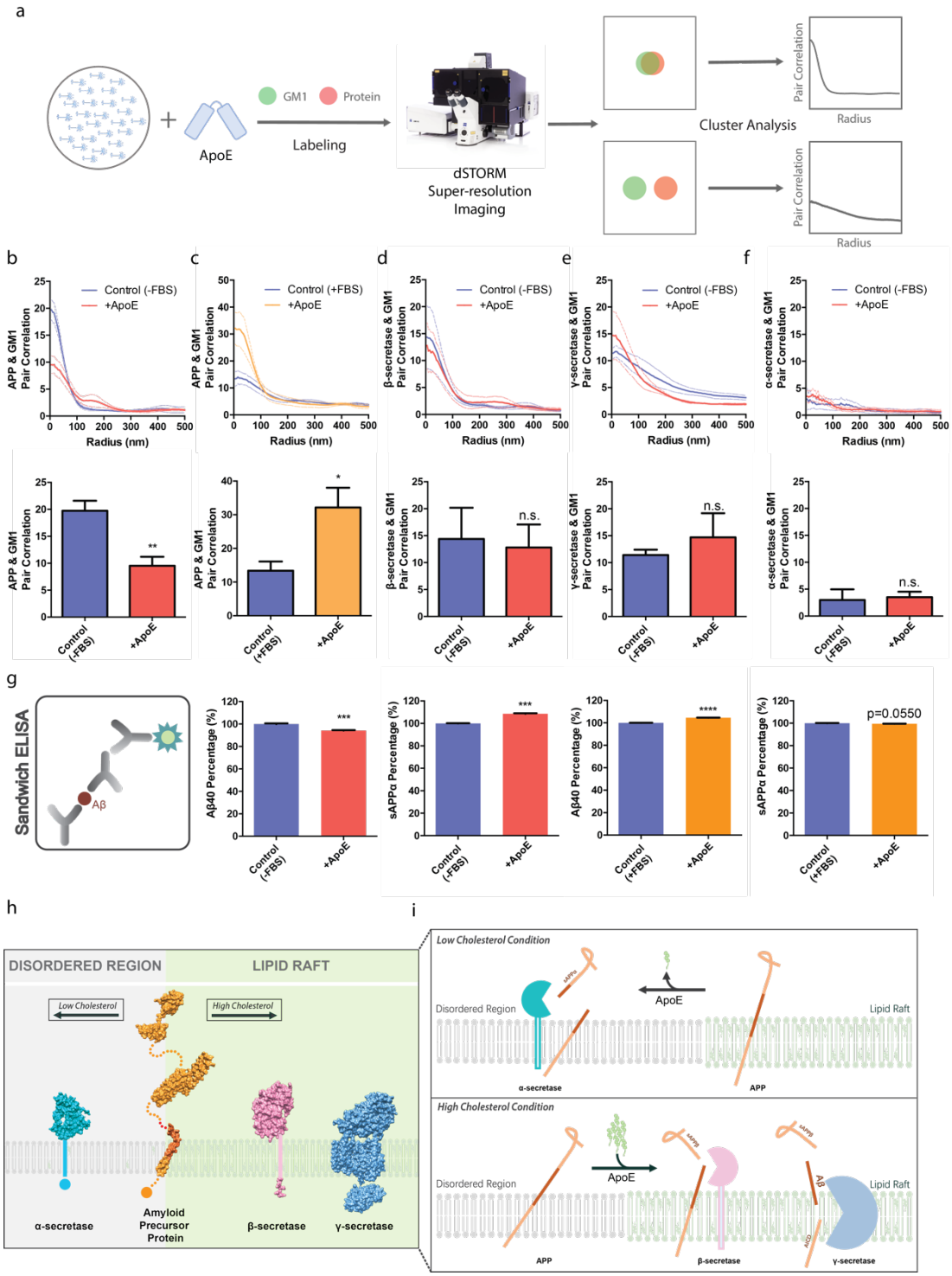

Figure 2. ApoE mediates APP's exposure to α- and β-secretase. (a) Workflow for dSTORM super-resolution. Cultured N2a cells (blue) are depicted in a dish (black circle). Cells were exposed to apoE (blue rectangles) with and without serum supplementation and fixed. GM1 lipids and amyloid proteins were fluorescently labeled (CTxB and antibody respectively) and imaged with super resolution (dSTORM). The proximity of the two labels (shown as red and green circles) was then determined by cluster analysis. Idealized pair correlations are shown for objects that strongly co-localize (top) and weakly co-localize (bottom) at a given radius. Pair correlations are unitless with 1 being little to no correlation and >5 a value typically significant in our experimental conditions. (b) Under low cholesterol conditions (no FBS), APP co-localization with raft domains decreases markedly after apoE treatment.

(c) Under high cholesterol conditions (with FBS), apoE-mediated APP co-localization with raft domains increases (i.e., apoE induces APP to translocate into lipid rafts). (d, e) β-secretase and γ-secretase lipid raft localization do not respond to apoE-mediated raft modulation. (f) α-secretase sits in the disordered region (low correlation with lipid raft). (g) Sandwich ELISA assay showing a shift from Aβ to sAPPα production after apoE treatment under low cholesterol condition. When presented cholesterol, APP's increased exposure to β- and γ-secretases results in an increased Aβ production. Data are expressed as mean ± s.e.m. *P<0.05, **P<0.01, ***P<0.001, ****P<0.0001, two-sided Student's t-test. (h, i) Because of raft disruption mediated by apoE, APP is ejected from lipid rafts into disordered regions under low cholesterol conditions, exposing it to α-secretase to be cleaved into non-amyloidogenic sAPPα. With high environmental cholesterol, apoE induced raft stabilization mediates more APP to be translocated into lipid rafts and cleaved by β- and γ-secretase, producing amyloidogenic Aβ peptides.

of little or no pair correlation and consistent with its lack of affinity for DRMs[15].

Cellular regulation of APP exposure to α- and β-secretase by apoE.

We then tested the role of apoE in mediating delivery of cholesterol to cell membranes and its effect on Aβ production in neuroblastoma 2a (N2a) cells. We applied 4 μg/mL of human apoE subtype 3 (apoE3) purified from *E. coli* with and without FBS, and measured APP localization to lipid rafts with dSTORM. We found that when cells were loaded with cholesterol (apoE3 +FBS), APP association with GM1 domains was almost two-fold higher than when cholesterol was effluxed (-FBS) (Figure 2b-c). FBS alone (no apoE added) did not increase APP trafficking to rafts (Figure 2c), suggesting apoE is a specific and necessary mediator of cholesterol transport to the neuron. Moreover, apoE alone (under low cholesterol condition (-FBS)) decreased APP raft affinity—significantly less APP was associated with GM1 domains compared to control cells without apoE (Figure 2b), confirming apoE can both load and unload cholesterol in neuronal membranes depending on apoE lipidation state and the availability of cholesterol. Consistent with cholesterol efflux, MβCD treatment trafficked APP out of GM1 domains (Figure S2)[12,15].

Surprisingly, cholesterol loading nor unloading of N2a cells by apoE had a significant effect on α-, β-, or γ-secretase trafficking in or out of GM1 domains (Figure 2d-f, h-i). GM1 domains were analyzed pairwise for association with either α-, β-, or γ-secretase identical to APP. In contrast to APP, cholesterol unloading with apoE treatment was insufficient to traffic β-, or γ-secretase out of GM1 domains. Likewise, more cholesterol failed to increase the association of any of the secretases. α-Secretase, located in the disordered region remained in the disordered region (Figures 2d, S2h), while β- and γ- secretases, which were already in the lipid rafts, did not increase their association with GM1 lipids in cholesterol loaded cells. This suggests that in the plasma membrane a mobile substrate (APP) moves between relatively static enzymes (secretases). Figure 2i summarizes the substrate moving between the different secretases based on raft-associated apoE-dependent trafficking and the expected cleavage products based on localization. With low cholesterol apoE traffics APP to α-secretase generating more sAPPα (top panel). During high cholesterol apoE traffics APP to β- and γ-secretase which produce neurotoxic Aβ peptide (bottom panel).

The role of astrocyte cholesterol in regulating APP processing in cultured primary neurons.

Since astrocytes produce much of the cholesterol for neurons, we hypothesized that astrocytes could control Aβ production through cholesterol. To test this hypothesis, we cultured primary cortical cells from mouse embryos (E17). In a first culture, we isolated just the neurons by sorting the cells with live cell fluorescence activated cell sorting (FACS) with Thy1.2, a cell surface marker of mature neurons. In a second culture we selected for neurons,but did not remove contaminating astrocytes resulting in a mixed culture. All cultures were treated with or without apoE, fixed, and labeled with appropriate fluorophores—the neurons were then imaged with dSTORM. We confirmed the presence of astrocytes in our mixed culture by staining for glial fibrillary acidic protein (GFAP). Around 0.95% of the mixed cell population was labelled by the GFAP antibody (Figure S3f).

We found that efflux of cholesterol from purified cortical neurons (Thy1.2^{+}) by incubation with

human apoE (from *E. coli*) generated dramatically decreased (>2-fold) APP association with GM1 domains, demonstrating cholesterol depletion causes GM1 domains to release APP to the disordered region (Figure 3a) in primary neurons. However, when we mixed astrocytes with neurons, apoE had the exact opposite effect. GM1 domains sequestered APP, evident by a 2.5-fold increase in APP association with GM1 lipids (Figure 3b). This suggests apoE delivers cholesterol from the astrocytes to the neurons and increases GM1 domain affinity for APP. Similar imaging of the secretases showed they remained immobile with α-secretase in the disordered region and β-secretase in GM1 domains (See Figure S3). Thus, astrocyte derived cholesterol is a dominant signal that controls APP association with α- or β-secretase in the neuron, based on GM1 domain affinity.

To further establish astrocyte derived cholesterol as the regulator of APP association with secretases, we specifically knocked down cholesterol synthesis in astrocytes by knocking out the SREBP2 gene using a tamoxifen inducible Cre recombinase system (Figure S4a). SREBP2 is the master transcriptional regulator of the majority of enzymes involved in cholesterol synthesis. Mice with SREBP2 knocked out of astrocytes have reduced production of cholesterol in the astrocytes[46] (Figure S4b). We cultured cortical neurons along with astrocytes from E17 pups and treated them with 100 nM 4-hydroxytamoxifen for 2 days to induce knockout of astrocyte SREBP2. Three days after 4-hydroxytamoxifen removal the cells were fixed and labeled, and APP localization was imaged with dSTORM, identical to the FACS sorted neurons above (see diagrams Figure 3).

Figure 3c shows a highly significant decrease in APP pair correlation with GM1 domains in mixed cultures containing SREBP2 (-/-) astrocytes, similar to purified Thy1.2 positive neuronal cultures (Figure 3c). Control cells from Thy1.2^{+} neurons and SREBP2 (-/-) neuron/astrocyte cultures were very similar, the amplitude of pair correlation was ~10 for both cultures. 4-hydoxytamoxifen treatment did not significantly alter APP GM1 pair correlation in the absence of Cre recombinase (Figure S4c).

We next examined if astrocytes contribute cholesterol to promote APP presence in neuronal lipid rafts *in vivo*. Astrocyte cholesterol synthesis was disrupted in mice by crossing SREBP2 floxed mice to GFAP-Cre mice resulting in a homyzgous deletion in SREBP2 in astrocyte cells [46]. At four weeks of age, brains were collected and APP-GM1 pair correlation was determined in neurons by dSTORM imaging. SREBP2 deletion in astrocytes resulted in a robust and significant reduction of APP-GM1 pair correlation compared to littermate controls (Figure 3d). This suggests that astrocyte cholesterol synthesis plays an essential role in maintaining cholesterol content in neuronal lipid rafts. These data further confirmed that astrocyte-derived cholesterol regulates APP translocation and association with secretases in the plasma membrane of neurons. Neurons appear incapable of increasing cholesterol synthesis to compensate for astrocyte deficiency in any appreciable way. Microglia also produce apoE in the brain[47], but they were also unable to completely compensate for a lack of astrocyte cholesterol synthesis.

The *in vivo* role of astrocyte cholesterol on Aβ and plaque formation in mouse brain.

As mentioned above, cholesterol is high in AD brains. Our model predicts attenuation of cholesterol in astrocytes should reduce the concentration of Aβ peptide formed *in vivo*. To test this hypothesis and to investigate the effect of astrocyte cholesterol on Aβ plaque formation in the intact brain we crossed 3xTg-AD mice, a well-established mouse model of AD[48], with our SREBP2$^{flox/flox}$ hGFAP-Cre mice[46] to generate an AD mouse model lacking astrocyte cholesterol. *In vivo*, Aβ exists in several forms, with Aβ1-40 being the most abundant and Aβ1-42 most closely associated with Alzheimer's disease pathology. The 3xTg-AD mouse expresses transgenes for mutant human APP and mutation in the presenilin 1 enzyme, both of which cause a significant increase in Aβ42 production.

Using an ELISA method to detect both human APP transgene derived Aβ40 and Aβ42, we measured both the RIPA soluble and insoluble

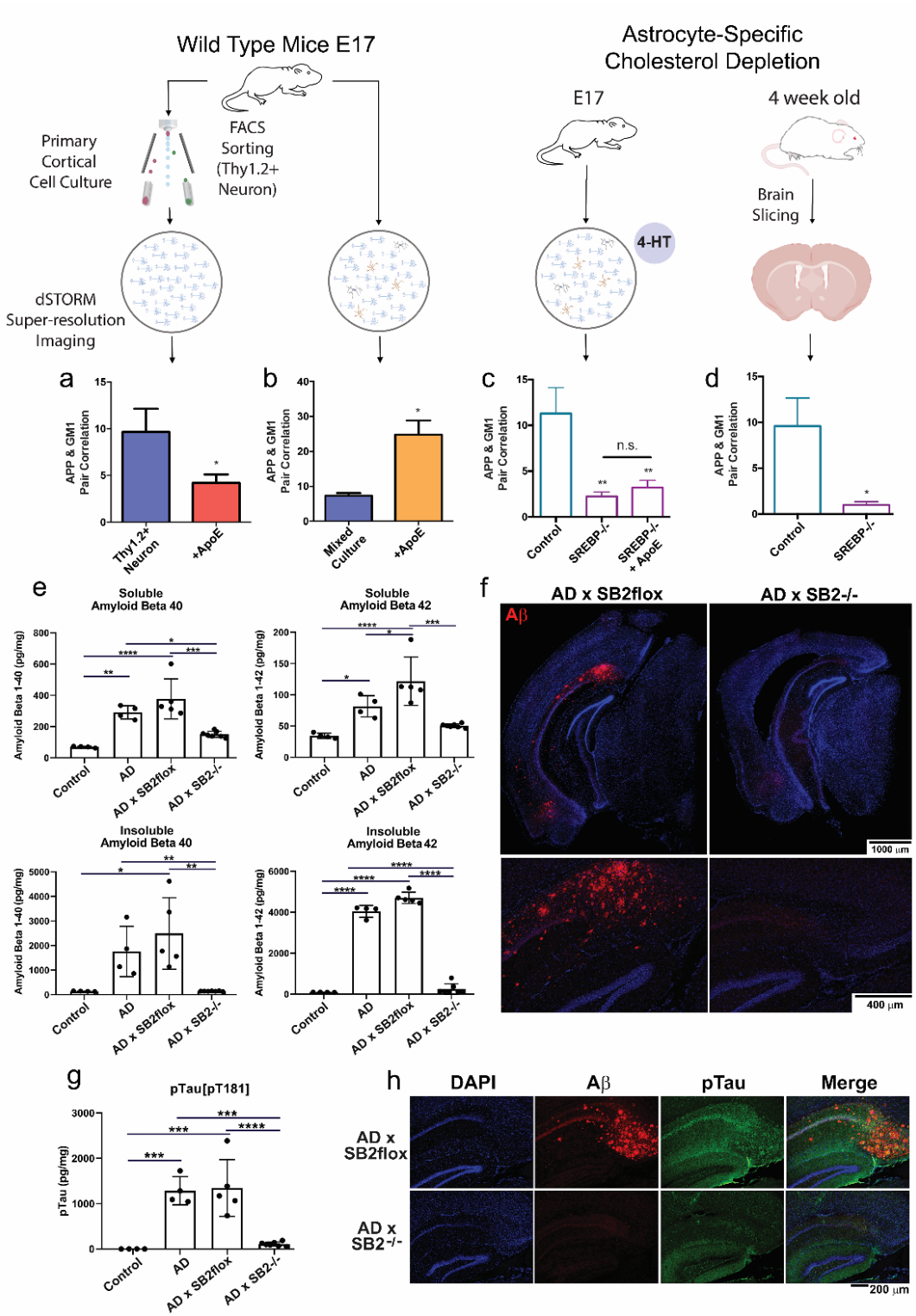

Figure 3. Astrocytes provide cholesterol for apoE's regulation of APP processing. Cortical cells were isolated from embryonic day 17 mice and cultured for dSTORM imaging. (a) ApoE translocates APP from lipid rafts into disordered regions in pure neuronal population sorted with cell surface neuronal marker Thy1.2. (b) ApoE increases APP's raft localization in primary neurons cultured in mixed population with glia cells including astrocytes. Data are expressed as mean ± s.e.m., n=3-10. *P<0.05, two-sided Student's t-test. (c) Astrocyte-specific cholesterol depletion completely disrupts APP raft localization in neurons in cultured cells. (d) Astrocyte cholesterol depletion

disrupts APP raft localization *in vivo* as demonstrated in SREBP2$^{flox/flox}$GFAP-Cre$^{+/-}$ mouse brain slices. Data are expressed as mean ± s.e.m., n=3-10. **P<0.01, one-way ANOVA. (e-h) 3xTg-AD mice (AD) were crossed to SREBP2$^{flox/flox}$GFAP-Cre$^{+/-}$ mice (AD x SB2$^{-/-}$) and aged to 60-weeks. (e) Hippocampus were isolated and soluble (RIPA-extracted) and insoluble (guanidine-extracted) amyloid-beta 40 and 42 species were measured by Elisa assay. Data are expressed as mean ± s.e.m, n=4-7. *P<0.05, **P<0.01, ***P<0.001, ****P<0.0001, one-way ANOVA with Tukey's post hoc analysis. (f) 60-week-old brain slices stained for human amyloid beta (red) and dapi (blue) in AD x SB2flox mice (left) and AD x SB2-/- mice (right). (g) pTau (phosphorylated threonine 181) levels were measured in 60-week-old hippocampus lysate by Elisa assay. Data are expressed as mean ± s.e.m, n=4-7. ***P<0.001, ****P<0.0001, one-way ANOVA with Tukey's post hoc analysis (h) 60-week-old brain slices were immunostained for pTau (green) and amyloid beta (red) and the subiculum region of the hippocampus was imaged.

fractions in the hippocampus of aged control and transgenic AD mice. Hippocampus tissue from wild type control mice was assessed to determine the nonspecific background of the Aβ signal in each ELISA assay. Knockout of SREBP2 in astrocytes of 3xTg-AD mice (AD x SB2-/-) reduced soluble Aβ40 and Aβ42 generation in hippocampus of 60-week-old mice by 2-fold, to levels only slightly higher than wildtype controls (Figure 3e) suggesting a near complete loss of amyloidogenic processing of APP. More impressively, insoluble Aβ40 and Aβ42 were almost entirely eliminated from AD x SB-/- hippocampus when assessed by ELISA assay (Figure 3e). This was verified by immunofluorescence staining demonstrating absence of amyloid plaques in AD x SB-/- mice (Figure 3f). Of note, total APP transgene expression was not impacted by loss of astrocyte SREBP2 (Figure S7). The 3xTg-AD model also expresses a transgene for human tau protein, another key component of Alzheimer's pathology. Tau is hyperphosphorylated in Alzheimer's disease and this is thought to be downstream of amyloid-beta accumulation[49]. It has also been proposed that cholesterol directly regulates tau phosphorylation [50,51]. In agreement with both of these hypotheses, phosphorylation of tau at the key T181 residue, but not total tau, is eliminated *in vivo* in the AD x SB-/- hippocampus (Figure 3g-h and Figure S7).

Activation of astrocytes cholesterol synthesis by inflammatory cytokines.

The specific role of astrocytes on APP localization and Aβ plaque formation led us to consider additional signals in disease states that might work through astrocytes to upregulate their formation. Among likely regulators, inflammation is a prominent risk factor associated with AD[52]. Neuroinflammation is characterized by the release of pro-inflammatory cytokines including interleukin 1β (IL1β), interleukin 6 (IL6) and tumor necrosis factor α (TNFα). These same cytokines are known to increase cholesterol production in peripheral tissues through SREBP2 activation[53–56], but their effects on astrocytes have not been tested.

To test the impact of inflammation on astrocyte cholesterol synthesis, we treated primary cultured astrocytes with IL1β, IL6 and TNFα. Primary astrocyte cultures were incubated for 1 hour with 1-100 ng/ml cytokines, then assayed for total cellular cholesterol with a fluorescent cholesterol assay (see methods). All the three cytokines dose dependently increased total levels of astrocyte cholesterol (up to 120%) (Figure 4a-c).

Figure 4d shows a proposed molecular mechanism for cholesterol regulation of Aβ formation. Inflammatory cytokines, possibly from microglia, activate astrocyte cholesterol synthesis. ApoE then loads cholesterol into neurons. Increased cholesterol in neurons drives APP to associate with β- and γ-secretases in lipid rafts, the association of APP with lipid rafts regulates the amount of Aβ formation, and Aβ levels dictate insoluble plaques.

DISCUSSION

While it has been known for some time that astrocytes play an important role in brain cholesterol production and express the AD genetic risk factor apoE, the role of astrocytes in AD pathogenesis remains poorly understood[57–59]. Astrocytes undergo robust morphological changes in neurodegenerative models and recent research demonstrates that astrocytes undergo broad transcriptional changes early in the AD process[60].

However, whether astrocytes are simply reacting to the AD neurodegenerative cascade or playing a role in promoting disease remains unclear. Here

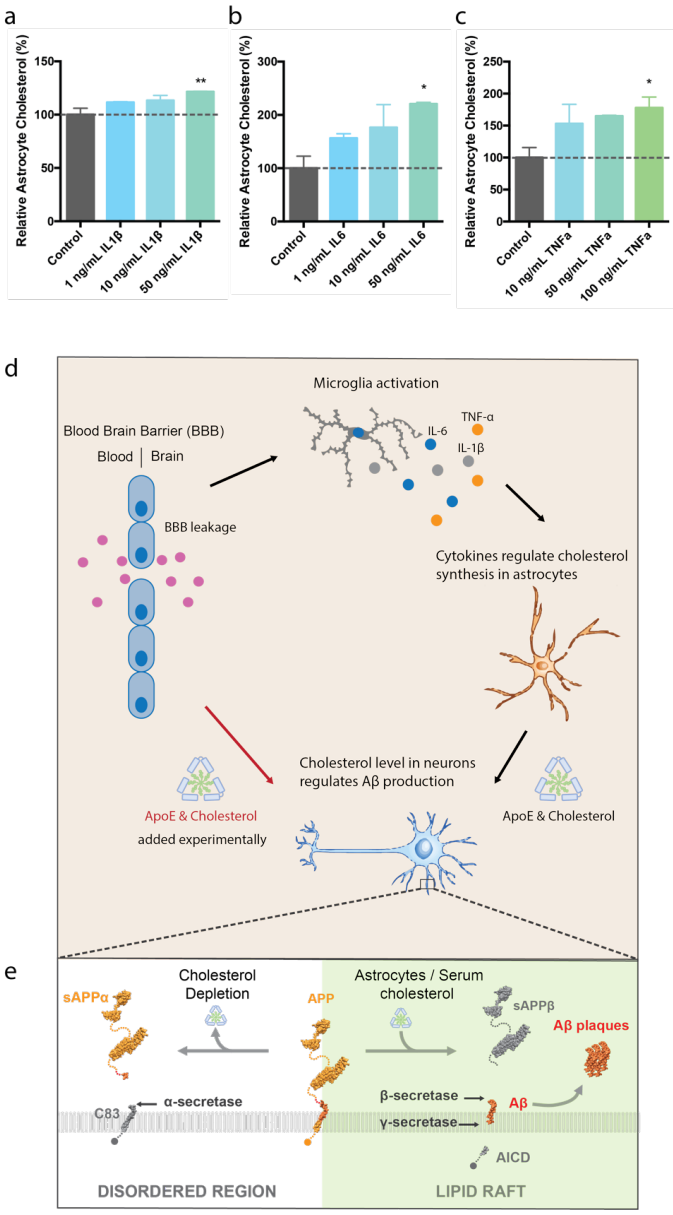

Figure 4. Pro-inflammatory cytokines induce cholesterol synthesis in astrocytes. (a) Interleukin-1β (IL-1β) induces cholesterol synthesis in primary cultured astrocytes dose dependently measured by a fluorescent based cholesterol assay. Data are expressed as mean ± s.e.m., *P<0.05, **P<0.01, one-way ANOVA. (b) Interleukin-6 (IL-6) induces cholesterol synthesis in primary cultured astrocytes. Data are expressed as mean ± s.e.m.. **P<0.01, two-sided Student's t-test. (d) A model is shown for a leaky blood brain barrier in Alzheimer's brain mediating inflammatory response in the central nervous system by activating microglia and inducing cytokine release. First, microglia-derived cytokines induce cholesterol synthesis in astrocytes. Then ApoE regulates neuronal Aβ production through astocyte cholesterol signaling. Adding apoE and blood derived cholesterol experimentally (red arrow) has a similar effect on neurons as astrocytes signaling through cholesterol. (e) The molecular mechanism for cholesterol regulation of Aβ in neurons. In low cholesterol (efflux) APP interacts α-secretase generating sAPPα. When cells are loaded with cholesterol, APP interacts with β- and γ-secretases generating Aβ plaques.

we demonstrate a direct role for astrocytes in promoting the AD phenotype through the production and distribution of cholesterol to neurons. Combined, our data established a molecular pathway that connects astrocyte cholesterol synthesis with apoE lipid trafficking and amyloidogenic processing of APP. The pathway establishes cholesterol as a critical lipid that controls the signaling state of a neuron. Cholesterol appears to be kept low as a mechanism to allow astrocytes to control GM1 raft function in the neuron. By keeping cholesterol low, the astrocyte can move the neuron through a concentration gradient that profoundly affects APP processing and eventual plaque formation. In essence cholesterol is set up to be used as a signaling lipid. Rather than targeting a receptor, it targets GM1 domains and sets the threshold for APP processing by altering GM1 domain function. This concept is likely important to other biological systems[61] given the profound effect of cholesterol on human health.

The rise and fall of Aβ peptide with cholesterol is striking, both in culture (Figure 2g) and *in vivo* (Figure 3e-f) and the data support the proposed molecular mechanism in which amyloidogenic processing of APP is promoted by cholesterol increasing APP interactions with β and γ secretases (Figure S1). This finding is in agreement with prior research implicating increased brain cholesterol content as a factor which promotes AD associated amyloid pathology. Administration of statins to guinea pigs has been shown to significantly reduce Aβ levels in the CSF[46]. APP/PS1 AD mice overexpressing a truncated active form of SREBP2 display an accelerated Aβ burden with aging[62]. Our findings contribute to literature demonstrating that amyloidogenic processing of APP in cultured cells occurs primarily in cholesterol rich membrane domains [15,63] and is consistent with cholesterol unloading decreasing Aβ formation in cell culture[64]. Cholesterol loading into cells appears to regulate more than just amyloid, it also appears to play an

essential role in the regulation of Tau[50]. We observed a striking reduction in levels of phosphorylated Tau in astrocyte SREBP2 knockout AD mice, which could result from reduced Aβ production or directly from cholesterol regulation. Our work is focused on cleavage of APP in neurons and primarily on the plasma membrane. Other mechanisms resulting from changes in brain cholesterol metabolism likely contribute to both amyloid production and clearance and require further investigation. Notwithstanding, astrocyte cholesterol is clearly a necessary signal for plaque formation even when APP is overexpressed.

The regulation of astrocyte cholesterol by cytokines is consistent with an antimicrobial function for Aβ (Figure 4d). The robust uprgulation of Aβ in response to blood derived cholesterol suggests a similar mechanism likely occurs in peripheral tissue or microhemmoraing in the brain. The coordinated regulation of Tau (Figure 2i) and Aβ (Figure 2e-f) may suggest an endogenous physiological function exists for this protein as well. The putative endogenous function of these proteins may explain why simply removing plaques was not as beneficial as expected in antibody-based treatments for AD[65].

At the molecular level, cholesterol loading regulates two functions: 1) the localization of the APP to GM1 domains and 2) the total number of GM1 domains (Figure 1e-f). Exactly how cholesterol is affecting GM1 domain function is not entirely clear. Palmitoylation drives raft association of the majority of integral raft proteins[8], but β, and γ-secretases are also palmitoylated and remain localized to GM1 lipids suggesting APP's exit involves additional factors that facilitate its release from GM1 domains. PIP_2 is a polyunsaturated lipid that resides in the disordered region and pulls PLD2 away from GM1 lipids[16]. If PIP_2 binds APP but not the secretases, this would help explain APP's selective trafficking away from GM1 lipids in low cholesterol. APP's localization to PIP_2 is not known, but PIP_2 is an important factor in AD[66,67].

Many channels are palmitoylated[68] and may respond to apoE and GM1 lipid domain function similar to APP. Investigating the effect of astrocyte cholesterol on channels will be important for studying AD since many of the palmitoylated channels have profound effects on neuronal excitability and learning and memory[68]. In a separate study we saw apoE and high cholesterol caused the potassium channel TREK-1 to traffic to lipid rafts similar to APP (Nayebosadri unpublished data)[69] and anesthetics[38] and mechanical force disrupts the localization[70].

Limitations of the Study. Clustering artifacts are a weakness of the study. CTxB is a pentadentate toxin that can cause artificial clustering[71]. Density-based spatial clustering of applications with noise (DBSCAN), a commonly used clustering analysis algorithm allows for an accurate comparison of relative size between apoE-treated and non-treated samples (Figure 4e), but does not necessarily correct artifacts in determining absolute size of the domain (Figure 4a)[72] (see also Figure S5 and Petersen et. al.[73] for clustering artifacts that can affect determining absolute size). The changes in size are described as 'apparent' for this reason. Hence, the effects of a treatment are limited to an observed change in size due to a specific treatment or condition. None of the conclusions from pair correlations (Figure 1-2) are affected by clustering. In fact, artificial clustering may help pair correlations by tightening the boundary of GM1-domains and allowing a better determination of a protein that is in or out of the domain.

Our data suggests cultured cells lacking apoE supplementation likely underestimate physiological GM1 domains size, especially those derived from the brain where cholesterol is high. Although it's only about 2% of the total body weight, the adult human brain contains up to 25% of all cholesterol in the body[74]. These high levels of cholesterol are likely missing in cultured cells. Not surprisingly, rafts appeared to be absent in cultured cells[71]. Not until cholesterol, supplied by astrocytes or cholesterol-containing apoE, was added were nanoscale rafts present (~100 nm). We conclude from our data, that the conditions with cholesterol are the more physiologically relevant conditions for cultured cells and 100 nm rafts are likely relevant to the *in vivo* function of many proteins.

Use of *in vivo* Cre-lox technology is always fraught with off-target deletions. In the case of targeting astrocytes, all astrocyte-targeting Cre lines also delete to some degree in neural progenitor cells. While our model also suffers from this short-coming, we have previously demonstrated that overall cholesterol synthesis by neurons increases

to compensate for loss of astrocyte cholesterol[46]. Thus, the dramatic decrease in Aβ and pTau that we observe in our cross of the 3xTg to the SREBP2$^{(-/-)}$-GFAP-Cre cannot readily be explained by the minority of knocked-out neurons. Rather, our data emphasize that the small changes in Aβ production we see in our cell culture models following acute treatment with cholesterol have a meaningful impact *in vivo,* where the cumulative impact of altering cholesterol delivery to neurons can be observed.

Lastly, our data largely support the reliability of DRM's as a first approximation of raft affinity[12,15]. Both dSTORM and DRMs found β, and γ-secretases firmly anchored in GM1 domains and α-secretase unassociated. Some have argued DRM's are not always identical to GM1 domains[12,75], and not surprisingly we see some slight differences. Compared to DRM, our data show APP associates more readily with GM1 domains. We suspect the addition of detergents in the preparation of DRM's causes some APP to leave GM1 rafts although we cannot rule out dSTORM introducing clustering artifacts that increase APP association with GM1 domains in dSTORM.

We conclude that the availability of astrocyte cholesterol regulates Aβ production by substrate presentation. This contributes to the understanding of AD and provides a potential explanation for the role of cholesterol associated genes as risk factors for AD.

METHODS

Animals

Housing, animal care and experimental procedures were consistent with the Guide for the Care and Use of Laboratory Animals and approved by the Institutional Animal Care and Use Committee of the Scripps Research Institute and the University of Virginia. 3xTg-AD mice and B6129SF2/J controls were purchased from Jackson labs. The 3xTg-AD mice were maintained homozygous for all transgenes. SREBP2$^{flox/flox}$ mice (a generous gift of Dr. Jay Horton at UT Southwestern, now available through Jackson labs) were crossed to the hGFAP-Cre as previously described[46]. These mice were in turn bred to the 3xTg-AD line and crossed back to homozygosity for both the 3xTg-AD transgenes and the SREBP2-flox. 3xTg-AD x SREBP2$^{flox/flox}$ (AD x SB2flox) and 3xTg-AD x SREBP2flox/flox x GFAP-Cre (AD x SB2$^{-/-}$) are littermates. Only female mice were used for the AD crosses as the male 3xTg-AD mice have a much milder phenotype.

Aldh1l1-Cre^{ERT2} mice were purchased from Jackson labs. These mice were crossed to the SREBP2$^{flox/flox}$ mice and the floxed allele was kept homozygous. Both male and female embryos were used from this mouse line.

Cell culture

Neuroblatoma 2a (N2a) cells and human embryonic kidney 293T (HEK293T) cells were grown in Dulbecco's Modified Eagle Medium (DMEM) containing 10% fetal bovine serum (FBS) and 1% penicillin/streptomycin. The cells were changed to a serum-free media 24 hours prior to experimentation unless otherwise noted.

Neurons were isolated from the cortices of embryonic day 18-21 CD1 mice. Cells were dissociated by papain digestion and plated on poly-D-lysine-coated (0.01 mg/mL) 8-well Lab-Tek II chambered cover glass (Thermo Fisher Scientific, #Z734853). Specifically, dissociated cells were plated in Minimum Essential Medium (MEM) supplemented with 5% FBS and 0.6% glucose and grown in Neurobasal medium (Thermo Fisher Scientific) supplemented with 20% B27 (Invitrogen), 1% Glutamax and 1% penicillin/streptomycin at 37 °C in 5% CO_2. Cells were cultured *in vitro* for two days prior to experiment. Astrocytes were cultured in DMEM containing 10% FBS and 1% penicillin/streptomycin as described previously[76].

Inducible Astrocyte SREBP2 Knockout Cultures

Astrocyte SREBP2 knockout cells with wild type neuron cocultures were grown by breeding ALDH1L1-Cre^{ERT2}xSREBP2$^{flox/flox}$ mice with SREBP2$^{flox/flox}$ mice. Embryonic day 17 brain cortices were harvested from embryos and cultured individually, while tails from each individual embryo were collected for determination of Cre genotyping. Meninges-free embryo cortices were digested in papain supplemented with DNAse

for 30 minutes then digestion was terminated by 4:1 addition of sterile HBSS + 20% fetal bovine serum. Following enzymatic dissociation, cells were centrifuged at 300 x g for 3 minutes. The resulting cell pellet was gently resuspended in plating media (MEM + 5% FBS + 0.6% glucose) using a 1mL pipette. Cells were plated on 0.01 mg/mL poly-d-lysine overnight coated Nunc™ Lab-Tek™ II 8-chambered coverglass or glass coverslips in plating media and placed in a 37-degree 5% CO2 cell culture incubator. After two hours, plating media was gently removed from the cells and replaced with neurobasal media supplemented with 20% B27 and 1% glutamax. After 4 days in culture, astrocyte SREBP2 ablation was induced by addition of 100 nM 4-OH Tamoxifen (Sigma-Aldrich H7904) to culture media for 48 hours. After 48 hours 4-OH tamoxifen was removed and media was replaced with fresh neurobasal media containing 20% B27 and 1% glutamax. Cells were then maintained in culture for 4 days and fixed for imaging as described below.

ApoE biosynthesis and purification

Recombinant human apoE protein was biosynthesized in HEK293T cells and purified to homogeneity as follows. To establish stable apoE-expressing cells, clone DNA of human apoE with C terminal FLAG tag (Sino Biological #HG10817-CF) was transfected into HEK293T cells using X-tremeGENE9 (Roche, #6365779001) as per the manufacturer's instructions. Stable pools were selected with 200 µg/mL Hygromycin B (Sigma-Aldrich, #H3274) for 2 weeks. Cell culture media containing secreted apoE protein was harvested and incubated with agarose beads column conjugating anti-FLAG antibody (anti-FLAG® M2 Affinity Gel, Sigma, #A2220) overnight at 4 °C. After incubation, the beads were washed thoroughly with 5 mL of protein reconstitution buffer (20 mM Tris-HCl, 150 mM NaCl, pH 7.5) three times before immunoprecipitated proteins were eluted with 75 µg FLAG peptide (Sigma, #F4799). Purified apoE protein was then delipidated by incubating with pre-equilibrated lipophilic hydroxyalkoxypropyl-dextran (Sigma, #H6383) overnight at room temperature with gentle rotation. Protein purity was assessed by Coomassie-stained sodium dodecyl sulfate–polyacrylamide gel electrophoresis (SDS-PAGE).

dSTORM Super-resolution imaging

Fixed cell preparation

N2a cells were grown to 60% confluence and then allowed to differentiate overnight in serum free media. Primary cortical cells were grown for two days *in vitro*. Cells were incubated with 4 µg/mL purified apoE protein for one day in media with or without FBS supplementation. Cells were rinsed with PBS and then fixed with 3% paraformaldehyde and 0.1% glutaraldehyde for 15 min to fix both proteins and lipids. Fixative chemicals were reduced by incubating with 0.1% $NaBH_4$ for 7 min with shaking followed by three times 10 min washes with PBS. Cells were permeabilized with 0.2% Triton X-100 for 15 min and then blocked with a standard blocking buffer (10% bovine serum albumin (BSA) / 0.05% Triton in PBS) for 90 min at room temperature. For labelling, cells were incubated with primary antibody for 60 min in 5% BSA / 0.05% Triton / PBS at room temperature followed by 5 washes with 1% BSA / 0.05% Triton / PBS for 15 min each. Secondary antibody was added in the same buffer as primary for 30 min at room temperature followed by 5 washes as stated above. Cells were then washed with PBS for 5 min. Cell labelling and washing steps were performed while shaking. Labeled cells were then post-fixed with fixing solution, as above, for 10 min without shaking followed by three 5 min washes with PBS and two 3 min washes with deionized distilled water.

Brain slice preparation

Mouse brain slicing and staining were performed as previously described[77] with minor modifications. Mouse brains were fixed in 4% paraformaldehyde, incubated in a 20% sucrose/PBS solution at 4 °C for 3 days, and embedded in Tissue-Tek OCT compound (Sakura). Sagittal sections (50 µm) were collected and placed into 24-well plate wells containing PBS. Fixative chemicals were reduced by incubating with 0.1% $NaBH_4$ for 30 min while gently shaking at room temperature followed by three times 10 min washes with PBS. Samples were permeabilized with 0.2% Triton X-100 for 2 hours and then blocked with a standard blocking buffer (10% bovine serum albumin (BSA) / 0.05% Triton in PBS) for 6 hours at room temperature. For

labelling, samples were incubated with primary antibody for 3 hours in 5% BSA / 0.05% Triton / PBS at room temperature then 3 days at 4 °C followed by 5 washes with 1% BSA / 0.05% Triton / PBS for 1 hour each. Secondary antibody was added in the same buffer as primary for 3 days at 4 °C followed by 5 washes as stated above. Sample labelling and washing steps were performed while shaking. Labeled brain tissues were then post-fixed with fixing solution, as above, for 1 hour without shaking followed by three 30 min washes with PBS and two 30 min washes with deionized distilled water. Brain slices were mounted onto the 35 mm glass bottom chamber (ibidi, #81158) and 2% agarose were pipetted onto the slice to form a permeable agarose pad and prevent sample movement during imaging.

dSTORM imaging

Images were recorded with a Zeiss ELYRA PS.1 microscope using TIRF mode equipped with a pil-immersion 63x objective. Andor iXon 897 EMCCD camera was used along with the Zen 10D software for image acquisition and processing. The TIRF mode in the dSTORM imaging provided low background high-resolution images of the membrane. A total of 10,000 frames with an exposure time of 18 ms were collected for each acquisition. Excitation of the Alexa Fluor 647 dye was achieved using 642 nm lasers and Cy3B was achieved using 561 nm lasers. Cells and brain tissues were imaged in a photo-switching buffer comprising of 1% β-mercaptoethanol (Sigma, #63689), and oxygen scavengers (glucose oxidase (Sigma, #G2133) and catalase (Sigma, #C40)) in 50mM Tris (Affymetrix, #22638100) + 10mM NaCl (Sigma, #S7653) + 10% glucose (Sigma, #G8270) at pH 8.0. Sample drift during acquisition was corrected by an autocorrelative algorithm.

Images were constructed using the default modules in the Zen software. Each detected event was fitted to a 2D Gaussian distribution to determine the center of each point spread function plus the localization precision. The Zen software also has many rendering options including removing localization errors and outliers based on brightness and size of fluorescent signals. Pair correlation and cluster analysis was performed using the Statistical Analysis package in the Vutara SRX software. Pair Correlation analysis is a statistical method used to determine the strength of correlation between two objects by counting the number of points of probe 2 within a certain donut-radius of each point of probe 1. This allows for localization to be determined without overlapping pixels as done in traditional diffraction-limited microscopy. Raft size estimation was calculated through cluster analysis by measuring the area of the clusters comprising of more than 10 particles with a maximum particle distance of 0.1 µm.

Fluorescence activated cell sorting (FACS) of live cells

Live cell staining for FACS was performed as previously described[78]. Immediately after dissection and dissociation, cortical cells from embryonic mice were labelled with Brilliant Violet 421™ anti-mouse CD90.2 (Thy1.2) antibody (BioLegend, #140327). Cells were incubated with antibody at 4 °C for 20 minutes followed by washing with wash buffer (Ca^{2+}/Mg^{2+} free PBS, 1mM EDTA, 25mM HEPES, 5% FBS, 10 units/mL DNase II). Cells were filtered through a 40-µm nylon filter (Corning, #431750) and sorted in a BD Biosciences FACSAria3 sorter. Thy1.2+ neurons were collected and cultured as described above.

Lipidomics

Lipidomics profiling was performed using Ultra Performance Liquid Chromatography-Tandem Mass Spectrometry (UPLC-MSMS).

Lipid extracts were prepared from cell preparations using modified Bligh and Dyer method, spiked with appropriate internal standards, and analyzed on a platform comprising Agilent 1260 Infinity HPLC integrated to Agilent 6490A QQQ mass spectrometer controlled by Masshunter v 7.0 (Agilent Technologies, Santa Clara, CA). Glycerophospholipids and sphingolipids were separated with normal-phase HPLC. An Agilent Zorbax Rx-Sil column (2.1 x 100 mm, 1.8 µm) maintained at 25°C was used under the following conditions: mobile phase A (chloroform: methanol: ammonium hydroxide, 89.9:10:0.1, v/v) and mobile phase B (chloroform: methanol: water: ammonium hydroxide, 55:39:5.9:0.1, v/v); 95% A for 2 min, decreased linearly to 30% A over 18 min and further decreased to 25% A over 3 min, before returning to 95% over 2 min and held for 6 min.

Separation of sterols and glycerolipids was carried out on a reverse phase Agilent Zorbax Eclipse XDB-C18 column (4.6 x 100 mm, 3.5um) using an isocratic mobile phase, chloroform, methanol, 0.1 M ammonium acetate (25:25:1) at a flow rate of 300 µl/min.

Quantification of lipid species was accomplished using multiple reaction monitoring (MRM) transitions under both positive and negative ionization modes in conjunction with referencing of appropriate internal standards: PA 14:0/14:0, PC 14:0/14:0, PE 14:0/14:0, PG 15:0/15:0, PI 17:0/20:4, PS 14:0/14:0, BMP 14:0/14:0, APG 14:0/14:0, LPC 17:0, LPE 14:0, LPI 13:0, Cer d18:1/17:0, SM d18:1/12:0, dhSM d18:0/12:0, GalCer d18:1/12:0, GluCer d18:1/12:0, LacCer d18:1/12:0, D7-cholesterol, CE 17:0, MG 17:0, 4ME 16:0 diether DG, D5-TG 16:0/18:0/16:0 (Avanti Polar Lipids, Alabaster, AL). Lipid levels for each sample were calculated by summing up the total number of moles of all lipid species measured by all three LC-MS methodologies.

Live raft affinity assay

Modulation of raft integrity was detected by a biochemical assay based on the activity of a palmitate mediated raft localized enzyme phospholipase D (PLD), as described previously[17]. Briefly, N2a cells were seeded into 96-well flat culture plates with transparent-bottom (Corning™ Costar™, #3585) to reach confluency (~ 5 x 10^4 per well). Then the confluent cells were differentiated with serum-free DMEM for a day and washed with 200 µL of phosphate buffer saline (PBS). The raft integrity assay reactions were promptly begun by adding 100 µL of working solution with or without apoE. ApoE3 (BioVision, #4696) and apoE4 (BioVision, 4699) were tested. The working solution contained 50 µM Amplex red, 1 U/mL horseradish peroxidase, 0.1 U/mL choline oxidase, and 30 µM dioctanoyl phosphatidylcholine (C8-PC). ApoE was directly dissolved into the working buffer from freshly made stocks before assay reagents were added. The PLD activity and the background (lacking cells) was determined in triplicate for each sample by measuring fluorescence activity with a fluorescence microplate reader (Tecan Infinite 200 PRO, reading from bottom) for 2 hours at 37°C with excitation wavelength of 530 nm and an emission wavelength of 585 nm. Subsequently, PLD activity was normalized by subtracting the background and to the control activity. Data were then graphed (Mean ± s.e.m.) and statistically analyzed (one-way ANOVA) with GraphPad Prism software (v6.0f).

Cholesterol assay

To measure the relative changes in cellular cholesterol level after apoE or cytokine treatment, we developed an Amplex Red-based cholesterol assay modified from the raft integrity assay described above. Briefly, N2a cells or astrocytes were seeded into 96-well flat culture plates with transparent-bottom to reach confluency (~ 5 x 10^4 per well). Then the confluent cells were differentiated with serum-free DMEM for a day. Cells were incubated with fresh DMEM for 1 hour followed by 1 hour of incubation in 100 µL of DMEM medium with or without treatment. Cytokines used in this study include: IL1β (Sigma-Aldrich, #SRP8033) and IL6 (Fisher, #PHC0064). After washing with 200 µL of PBS, cholesterol assay reactions were promptly begun by adding 100 µL of working solution containing 50 µM Amplex red, 1 U/mL horseradish peroxidase, 2 U/mL cholesterol oxidase and 2 U/mL cholesterul esterase in PBS. Relative cholesterol concentration and the background (lacking cells) was determined in triplicate for each sample by measuring fluorescence activity with a fluorescence microplate reader (Tecan Infinite 200 PRO, reading from bottom) for 2 hours at 37°C with excitation wavelength of 530 nm and an emission wavelength of 585 nm. Subsequently, cholesterol level was normalized by subtracting the background and to the control activity. End point cholesterol signals were then graphed (Mean ± s.e.m.) and statistically analyzed (one-way ANOVA) with GraphPad Prism software (v6.0f).

ELISA assay

To measure the relative changes in β- and α-cleavage products of APP, N2a cells were incubated with apoE with and without FBS supplementation for 1 hour, then washed with PBS once and incubated with PBS for 1 hour. Supernatant were harvested and analyzed with Aβ40 and sAPPα ELISAs.

Relative quantitation of secreted Aβ40 was performed with commercial human Aβ40 ELISA kit (Invitrogen, #KHB3481) following the manufacturer's instructions. For sAPPα ELISA, 5 µg/mL rabbit anti-APP antibody (abcam, #ab15272) was coated on immunoassay plates (Corning™ Costar™ Cell Culture 96 well plates, #3585) at 4 °C overnight. Then, the plates were washed with PBS three times. Next, 50 µL of supernatant was added and incubated at room temperature for 1 hour. After this, 50 µL of 2 µg/mL mouse anti-human sAPPα IgG monoclonal antibody (IBL, #11088) was added as primary detection antibody. After incubation for 3 hours at room temperature, the plates were washed with PBST buffer (PBS with 0.05% Tween-20) and then 100 µL of 100 ng/mL HRP-linked rabbit anti-mouse IgG secondary antibody (Invitrogen, #31450) was added and incubated for 1 hour. An HRP substrate, chromogen (Invitrogen, #KHB3481) was added and incubated at room temperature in the dark for 30 minutes. The substrate development was terminated by adding 100 µL of stop solution from ELISA kit (Invitrogen, #KHB3481). Relative sAPPα concentration was determined by measuring absorbance at 450 nm using a microplate reader (Tecan Infinite 200 PRO).

Confocal imaging on brain slices and primary cells

Mouse brains were fixed in 4% paraformaldehyde, incubated in a 20% sucrose/PBS solution at 4 °C for 3 days, and embedded in Tissue-Tek OCT compound (Sakura). Sagittal sections (50 µm) were collected on Superfrost/Plus slides and immunostained with mouse NF-M antibody (Santa Cruz, #sc-398532), Alexa Fluor-647-conjugated CTxB (Invitrogen, #C34778) and Cy3B-conjugated anti-mouse secondary antibody. Human amyloid beta was detected using a polyclonal antibody from Cell Signaling (#8243) with Alexa Fluor 594 anti-rabbit secondary (Thermo Fisher Scientific, #A21207). Primary cortical cells were fixed and labelled with Alexa Fluor-488-conjugated mouse GFAP antibody (Biolegend, #644704), or rabbit GFAP antibody (Millipore, #MAB360) with Alexa Fluor 594 anti-rabbit secondary (Thermo Fisher Scientific, #A21207). SREBP2 knockout was confirmed by measuring the downstream enzyme FDFT1 (Abcam, #ab195046, Alexa Fluor 488 secondary Thermo Fisher Scientific #A32766) pTau was imaged in brain sections using the mouse monoclonal AT180 antibody from Thermo Fisher Scuentific (#MN1040). Samples were imaged on Leica TCS SP8 confocal microscope using a 25× water emersion objective. ImageJ was used to analyze images.

Tissue Western Blots

40 week old mouse hippocampus tissue was homogenized in RIPA buffer with protease inhibitors using a Bullet Blender®. The homogenate was centrifuged at 15,000 x g for 10 minutes, and the supernatant was collected. Total protein content was measure using the pierce 660 absorbance assay. Sample protein content was diluted to equal concentrations, and Laemmli buffer (Biorad, 1610737) was added to each sample for SDS-Page. SDS-Page was performed to resolve protein by molecular weight using 10 micrograms of hippocampus lysate from each sample in 4-20% acrylamide pre-cast gels (Biorad, 4568094). Resolved protein was transferred to PVDF membrane and blocked with 5% BSA solution in PBST. Primary antibodies against target proteins were applied overnight at 4 degrees. Membranes were then washed and fluorescent secondary antibodies were applied for 2 hours at room temperature. Following 5 washes with TBS with 0.1% tween, membranes were imaged using the Bio Rad chemidoc MP fluorescent imaging system. Primary antibodies used in this study include: APP (Y188), Abcam, #ab32136; Tau, Fisher Scientific, #AHB0042; Cre, Biolegend, #908001; Actin, Biorad, #12004163.

Statistics

All statistical calculations were performed in GraphPad Prism v6.0. For the Student's t test, significance was calculated using a two-tailed unpaired parametric test with significance defined as $p < 0.05$, $^{**}P<0.01$, $^{***}P<0.001$, $^{****}P<0.0001$. For the multiple comparison test, significance was calculated using an ordinary one-way ANOVA with Dunnett's multiple comparisons test.

Acknowledgements

We thank Andrew S. Hansen and Damon Page for aspects of experimental design, E. Nicholas

Petersen for his help and discussion on the imaging and imaging analysis, Eddie Grinman and the Puthanveettil lab for mouse cortical tissue. We thank biomarker core (Columbia University, NY) and flow cytometry core (Scripps Research, FL) for technical support. This work was supported by the National Institutes of Health via a Director's New Innovator Award to S.B.H. (DP2NS087943), R01 to S.B.H. (R01NS112534), K08 (K08DK097293) to H.A.F., and T32 (T32DK764627) to J.A.K. We are grateful to the Iris and Junming Le Foundation for funds to purchase a super-resolution microscope, making this study possible.

Author Contributions

Conceptualization, S.B.H. and H.W.; Methodology, H.W., J.A.K., H.A.F. and S.B.H.; Investigation, H.W. and J.A.K; Resources, S.B.H. and H.A.F., Writing – Original Draft, H.W. and S.B.H.; Writing – Review and Editing, H.W., H.A.F., and S.B.H.; Supervision, H.A.F. and S.B.H.; Funding Acquisition, H.A.F. and S.B.H.

Competing Interests

The authors declare no competing interests.

REFERENCES

1. Haass, C. & Selkoe, D. J. Cellular processing of β-amyloid precursor protein and the genesis of amyloid β-peptide. *Cell* (1993). doi:10.1016/0092-8674(93)90312-E
2. Shokri-Kojori, E. *et al.* β-Amyloid accumulation in the human brain after one night of sleep deprivation. *Proc. Natl. Acad. Sci. U. S. A.* **115**, 4483–4488 (2018).
3. Xie, L. *et al.* Sleep drives metabolite clearance from the adult brain. *Science* **342**, 373–7 (2013).
4. Gosztyla, M. L., Brothers, H. M. & Robinson, S. R. Alzheimer's Amyloid-β is an Antimicrobial Peptide: A Review of the Evidence. *Journal of Alzheimer's Disease* (2018). doi:10.3233/JAD-171133
5. Rice, H. C. *et al.* Secreted amyloid-b precursor protein functions as a GABA B R1a ligand to modulate synaptic transmission. *Science (80-.).* **363**, (2019).
6. Chow, V. W., Mattson, M. P., Wong, P. C. & Gleichmann, M. An overview of APP processing enzymes and products. *Neuromolecular medicine* (2010). doi:10.1007/s12017-009-8104-z
7. Marzolo, M. P. & Bu, G. Lipoprotein receptors and cholesterol in APP trafficking and proteolytic processing, implications for Alzheimer's disease. *Seminars in Cell and Developmental Biology* (2009). doi:10.1016/j.semcdb.2008.10.005
8. Levental, I., Lingwood, D., Grzybek, M., Coskun, U. & Simons, K. Palmitoylation regulates raft affinity for the majority of integral raft proteins. *Proc. Natl. Acad. Sci.* **107**, 22050–22054 (2010).
9. Vetrivel, K. S. & Thinakaran, G. Membrane rafts in Alzheimer's disease beta-amyloid production. *Biochimica et Biophysica Acta - Molecular and Cell Biology of Lipids* **1801**, 860–867 (2010).
10. Araki, W. Post-translational regulation of the β-secretase BACE1. *Brain Research Bulletin* **126**, 170–177 (2016).
11. Bhattacharyya, R., Barren, C. & Kovacs, D. M. Palmitoylation of amyloid precursor protein regulates amyloidogenic processing in lipid rafts. *J. Neurosci.* **33**, 11169–11183 (2013).
12. Cordy, J. M., Hooper, N. M. & Turner, A. J. The involvement of lipid rafts in Alzheimer's disease (review). *Molecular Membrane Biology* **23**, 111–122 (2006).
13. Vetrivel, K. S. *et al.* Alzheimer disease Aβ production in the absence of S-palmitoylation-dependent targeting of BACE1 to lipid rafts. *J. Biol. Chem.* (2009). doi:10.1074/jbc.M808920200
14. Cheng, H. *et al.* S-Palmitoylation of γ-secretase subunits nicastrin and aph-1. *J. Biol. Chem.* (2009). doi:10.1074/jbc.M806380200
15. Ehehalt, R., Keller, P., Haass, C., Thiele, C. & Simons, K. Amyloidogenic processing of the Alzheimer β-amyloid precursor protein depends on lipid rafts. *J. Cell Biol.* **160**, 113–123 (2003).
16. Robinson, C. V., Rohacs, T. & Hansen, S. B. Tools for Understanding Nanoscale Lipid Regulation of Ion Channels. *Trends Biochem. Sci.* **44**, 795–806 (2019).
17. Petersen, E. N., Chung, H.-W., Nayebosadri, A. & Hansen, S. B. Kinetic disruption of lipid rafts is a mechanosensor for phospholipase D. *Nat. Commun.* **7**, 13873 (2016).
18. Di Paolo, G., Kim, T. W. & Paolo, G. Di. Linking lipids to Alzheimer's disease: cholesterol and beyond. *Nat. Rev. Neurosci.* **12**, 284–96 (2011).
19. Reitz, C. Dyslipidemia and dementia: Current epidemiology, genetic evidence, and mechanisms behind the associations. *Journal of Alzheimer's Disease* (2012). doi:10.3233/JAD-2011-110599
20. Gamba, P. *et al.* The link between altered cholesterol metabolism and Alzheimer's disease. *Ann. N. Y. Acad. Sci.* (2012). doi:10.1111/j.1749-6632.2012.06513.x
21. Zhao, J. *et al.* β-Secretase processing of the β-amyloid precursor protein in transgenic mice is efficient in neurons but inefficient in astrocytes. *J. Biol. Chem.* (1996). doi:10.1074/jbc.271.49.31407

22. Calhoun, M. E. *et al.* Neuronal overexpression of mutant amyloid precursor protein results in prominent deposition of cerebrovascular amyloid. *Proc. Natl. Acad. Sci. U. S. A.* (1999). doi:10.1073/pnas.96.24.14088
23. Quan, G., Xie, C., Dietschy, J. M. & Turley, S. D. Ontogenesis and regulation of cholesterol metabolism in the central nervous system of the mouse. *Dev. Brain Res.* (2003). doi:10.1016/j.devbrainres.2003.09.015
24. Dietschy, J. M. & Turley, S. D. Cholesterol metabolism in the central nervous system during early development and in the mature animal. *Journal of Lipid Research* (2004). doi:10.1194/jlr.R400004-JLR200
25. Russell, D. W., Halford, R. W., Ramirez, D. M. O., Shah, R. & Kotti, T. Cholesterol 24-Hydroxylase: An Enzyme of Cholesterol Turnover in the Brain. *Annu. Rev. Biochem.* (2009). doi:10.1146/annurev.biochem.78.072407.103859
26. Vance, J. E. & Hayashi, H. Formation and function of apolipoprotein E-containing lipoproteins in the nervous system. *Biochimica et Biophysica Acta - Molecular and Cell Biology of Lipids* (2010). doi:10.1016/j.bbalip.2010.02.007
27. Strittmatter, W. J. *et al.* Apolipoprotein E: High-avidity binding to β-amyloid and increased frequency of type 4 allele in late-onset familial Alzheimer disease. *Proc. Natl. Acad. Sci. U. S. A.* **90**, 1977–1981 (1993).
28. Corder, E. H. *et al.* Gene dose of apolipoprotein E type 4 allele and the risk of Alzheimer's disease in late onset families. *Science (80-.).* **261**, 921–923 (1993).
29. Lingwood, D. & Simons, K. Lipid rafts as a membrane-organizing principle. *Science* **327**, 46–50 (2010).
30. Sezgin, E., Levental, I., Mayor, S. & Eggeling, C. The mystery of membrane organization: composition, regulation and roles of lipid rafts. *Nat. Rev. Mol. Cell Biol.* **18**, 361–374 (2017).
31. van den Bogaart, G. *et al.* Membrane protein sequestering by ionic protein-lipid interactions. *Nature* **479**, 552–5 (2011).
32. Wang, J. & Richards, D. a. Segregation of PIP2 and PIP3 into distinct nanoscale regions within the plasma membrane. *Biol. Open* **1**, 857–62 (2012).
33. Jones, S. a, Shim, S.-H., He, J. & Zhuang, X. Fast, three-dimensional super-resolution imaging of live cells. *Nat. Methods* **8**, 499–508 (2011).
34. Huang, B., Wang, W., Bates, M. & Zhuang, X. Three-dimensional super-resolution imaging by stochastic optical reconstruction microscopy. *Science* **319**, 810–3 (2008).
35. Betzig, E. *et al.* Imaging intracellular fluorescent proteins at nanometer resolution. *Science* **313**, 1642–1645 (2006).
36. Hess, S. T., Girirajan, T. P. K. K. & Mason, M. D. Ultra-high resolution imaging by fluorescence photoactivation localization microscopy. *Biophys. J.* **91**, 4258–4272 (2006).
37. Honigmann, A. *et al.* Scanning STED-FcS reveals spatiotemporal heterogeneity of lipid interaction in the plasma membrane of living cells. *Nat. Commun.* **5**, (2014).
38. Pavel, M. A., Petersen, E. N., Wang, H., Lerner, R. A. & Hansen, S. B. Studies on the mechanism of general anesthesia. *Proc. Natl. Acad. Sci.* 202004259 (2020). doi:10.1073/pnas.2004259117
39. Hua, X. *et al.* SREBP-2, a second basic-helix-loop-helix-leucine zipper protein that stimulates transcription by binding to a sterol regulatory element. *Proc. Natl. Acad. Sci. U. S. A.* **90**, 11603–11607 (1993).
40. Srinivasan, R. *et al.* New Transgenic Mouse Lines for Selectively Targeting Astrocytes and Studying Calcium Signals in Astrocyte Processes In Situ and In Vivo. *Neuron* **92**, 1181–1195 (2016).
41. Luo, J., Yang, H. & Song, B. L. Mechanisms and regulation of cholesterol homeostasis. *Nat. Rev. Mol. Cell Biol.* **21**, 225–245 (2020).
42. Chen, J., Zhang, X., Kusumo, H., Costa, L. G. & Guizzetti, M. Cholesterol efflux is differentially regulated in neurons and astrocytes: Implications for brain cholesterol homeostasis. *Biochimica et Biophysica Acta - Molecular and Cell Biology of Lipids* **1831**, 263–275 (2013).
43. Hayashi, H., Campenot, R. B., Vance, D. E. & Vance, J. E. Apolipoprotein E-containing lipoproteins protect neurons from apoptosis via a signaling pathway involving low-density lipoprotein receptor-related protein-1. *J. Neurosci.* **27**, 1933–1941 (2007).
44. Lindh, M. *et al.* Cerebrospinal fluid apolipoprotein E (apoE) levels in Alzheimer's disease patients are increased at follow up and show a correlation with levels of tau protein. *Neurosci. Lett.* (1997). doi:10.1016/S0304-3940(97)00429-1
45. Zidovetzki, R. & Levitan, I. Use of cyclodextrins to manipulate plasma membrane cholesterol content: Evidence, misconceptions and control strategies. *Biochimica et Biophysica Acta - Biomembranes* (2007). doi:10.1016/j.bbamem.2007.03.026
46. Ferris, H. A. *et al.* Loss of astrocyte cholesterol synthesis disrupts neuronal function and alters whole-body metabolism. *Proc. Natl. Acad. Sci. U. S. A.* **114**, 1189–1194 (2017).
47. Liu, C.-C. C.-C., Liu, C.-C. C.-C., Kanekiyo, T., Xu, H. & Bu, G. Apolipoprotein E and Alzheimer disease: risk, mechanisms and therapy. *Nat. Rev. Neurol.* **9**, 106–18 (2013).
48. Oddo, S. *et al.* Triple-transgenic model of Alzheimer's disease with plaques and tangles: intracellular Abeta and synaptic dysfunction. *Neuron* **39**, 409–421 (2003).
49. Selkoe, D. J. & Hardy, J. The amyloid hypothesis of Alzheimer's disease at 25 years. *EMBO Mol. Med.* **8**, 595–

608 (2016).
50. van der Kant, R. *et al.* Cholesterol Metabolism Is a Druggable Axis that Independently Regulates Tau and Amyloid-β in iPSC-Derived Alzheimer's Disease Neurons. *Cell Stem Cell* **24**, 363-375.e9 (2019).
51. van der Kant, R., Goldstein, L. S. B. & Ossenkoppele, R. Amyloid-β-independent regulators of tau pathology in Alzheimer disease. *Nat. Rev. Neurosci.* **21**, 21–35 (2020).
52. Kinney, J. W. *et al.* Inflammation as a central mechanism in Alzheimer's disease. *Alzheimer's Dement. Transl. Res. Clin. Interv.* **4**, 575–590 (2018).
53. Tumurkhuu, G. *et al.* Chlamydia pneumoniae Hijacks a Host Autoregulatory IL-1β Loop to Drive Foam Cell Formation and Accelerate Atherosclerosis. *Cell Metab.* (2018). doi:10.1016/j.cmet.2018.05.027
54. Gierens, H. *et al.* Interleukin-6 stimulates LDL receptor gene expression via activation of sterol-responsive and Sp1 binding elements. *Arterioscler. Thromb. Vasc. Biol.* (2000). doi:10.1161/01.ATV.20.7.1777
55. Stopeck, A. T., Nicholson, A. C., Mancini, F. P. & Hajjar, D. P. Cytokine regulation of low density lipoprotein receptor gene transcription in HepG2 cells. *J. Biol. Chem.* (1993).
56. Tacer, K. F., Kuzman, D., Seliškar, M., Pompon, D. & Rozman, D. TNF-α interferes with lipid homeostasis and activates acute and proatherogenic processes. *Physiol. Genomics* (2007). doi:10.1152/physiolgenomics.00264.2006
57. Mauch, D. H. *et al.* CNS synaptogenesis promoted by glia-derived cholesterol. *Science* **294**, 1354–1357 (2001).
58. LaDu, M. J. *et al.* Nascent astrocyte particles differ from lipoproteins in CSF. *J. Neurochem.* **70**, 2070–2081 (1998).
59. Boyles, J. K., Pitas, R. E., Wilson, E., Mahley, R. W. & Taylor, J. M. Apolipoprotein E associated with astrocytic glia of the central nervous system and with nonmyelinating glia of the peripheral nervous system. *J. Clin. Invest.* **76**, 1501–1513 (1985).
60. Habib, N. *et al.* Disease-associated astrocytes in Alzheimer's disease and aging. *Nat. Neurosci.* (2020). doi:10.1038/s41593-020-0624-8
61. Wang, H., Yuan, Z., Pavel, M. A. & Hansen, S. The role of high cholesterol in aged related COVID19 lethality. *bioRxiv* 2020.05.09.086249 (2020). doi:10.1101/2020.05.09.086249
62. Barbero-Camps, E., Fernandez, A., Martinez, L., Fernandez-Checa, J. C. & Colell, A. APP/PS1 mice overexpressing SREBP-2 exhibit combined Abeta accumulation and tau pathology underlying Alzheimer's disease. *Hum. Mol. Genet.* **22**, 3460–3476 (2013).
63. Puglielli, L., Tanzi, R. E. & Kovacs, D. M. Alzheimer's disease: the cholesterol connection. *Nat. Neurosci.* **6**, 345–351 (2003).
64. Sano, O. *et al.* ABCG1 and ABCG4 suppress γ-secretase activity and amyloid β production. *PLoS One* **11**, 1–19 (2016).
65. Selkoe, D. J. Alzheimer disease and aducanumab: adjusting our approach. *Nature Reviews Neurology* **15**, 365–366 (2019).
66. Berman, D. E. *et al.* Oligomeric amyloid-β peptide disrupts phosphatidylinositol-4,5- bisphosphate metabolism. *Nat. Neurosci.* **11**, 547–554 (2008).
67. Landman, N. *et al.* Presenilin mutations linked to familial Alzheimer's disease cause an imbalance in phosphatidylinositol 4,5-bisphosphate metabolism. *Proc. Natl. Acad. Sci. U. S. A.* **103**, 19524–19529 (2006).
68. Shipston, M. J. Ion channel regulation by protein palmitoylation. *J. Biol. Chem.* **286**, 8709–8716 (2011).
69. Nayebosadri, A., Petersen, E. N., Cabanos, C. & Hansen, S. B. A Membrane Thickness Sensor in TREK-1 Channels Transduces Mechanical Force. *SSRN Electron. J.* (2018). doi:10.2139/ssrn.3155650
70. Petersen, E. N. *et al.* Phospholipase D Transduces Force to TREK-1 Channels in a Biological Membrane. 758896 (2019). doi:10.1101/758896
71. Moon, S. *et al.* Spectrally Resolved, Functional Super-Resolution Microscopy Reveals Nanoscale Compositional Heterogeneity in Live-Cell Membranes. *J. Am. Chem. Soc.* **139**, 10944–10947 (2017).
72. Veatch, S. L. *et al.* Correlation functions quantify super-resolution images and estimate apparent clustering due to over-counting. *PLoS One* **7**, (2012).
73. Petersen, E. N., Pavel, M. A., Wang, H. & Hansen, S. B. Disruption of palmitate-mediated localization; a shared pathway of force and anesthetic activation of TREK-1 channels. *Biochim. Biophys. Acta - Biomembr.* **1862**, 183091 (2020).
74. Reiss, A. B. *et al.* Cholesterol in neurologic disorders of the elderly: Stroke and Alzheimer's disease. *Neurobiology of Aging* (2004). doi:10.1016/j.neurobiolaging.2003.11.009
75. Lichtenberg, D., Goñi, F. M. & Heerklotz, H. Detergent-resistant membranes should not be identified with membrane rafts. *Trends Biochem. Sci.* **30**, 430–436 (2005).
76. Schildge, S., Bohrer, C., Beck, K. & Schachtrup, C. Isolation and culture of mouse cortical astrocytes. *J. Vis. Exp.* (2013). doi:10.3791/50079
77. German, C. L., Gudheti, M. V., Fleckenstein, A. E. & Jorgensen, E. M. Brain slice staining and preparation for three-dimensional super-resolution microscopy. in *Methods in Molecular Biology* (2017). doi:10.1007/978-1-4939-7265-4_13

78. Schwarz, J. M. Using fluorescence activated cell sorting to examine cell-type-specific gene expression in rat brain tissue. *J. Vis. Exp.* (2015). doi:10.3791/52537

SUPPLEMENTAL FIGURES

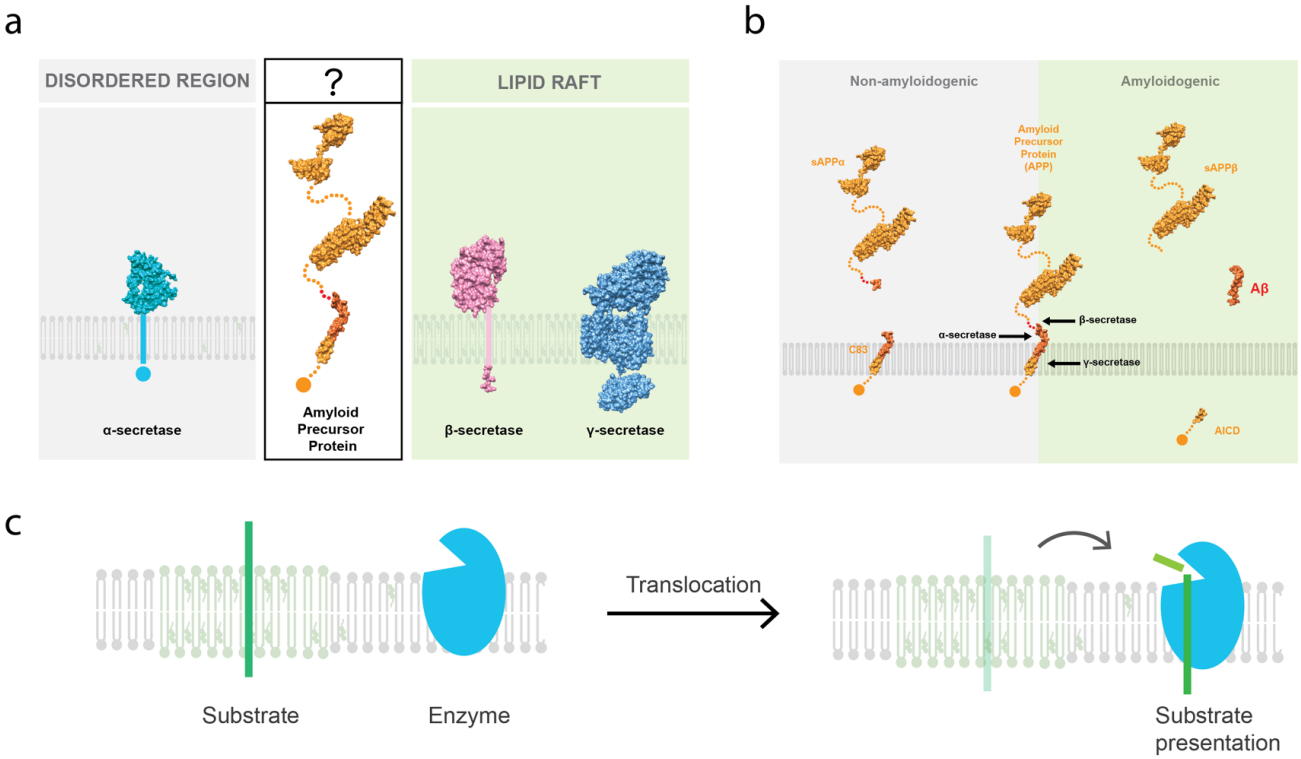

Figure S1. Amyloid proteins and substrate presentation. (a) The atomic structures of amyloid proteins and their predicted sub-membrane localizations based on palmitate mediated localization. Amyloid precursor protein (APP) and β- and γ-secretases are palmitoylated on their N-terminus. The palmitoylation is known to cause partitioning into detergent resistant membrane and raft-associated (green shading). α-Secretase is not palmitoylated and expected to reside in the disordered regions (grey shading). (b) The known APP cleavage sites for APP-processing proteins. In general, the α-secretase or β-secretase cleaves the APP extracellular domain generating the soluble N-terminal fragments (e.g. sAPPα or sAPPβ) and membrane-associated C-terminal fragments (CTF). CTFβ is further cleaved by the γ-secretase within the transmembrane domain releasing p3 peptide or β-amyloid (Aβ) peptide (respectively). (c) Substrate presentation is a biological process that activates a protein. The protein is sequestered away from its substrate and then activated by release and exposure of the protein to its substrate.

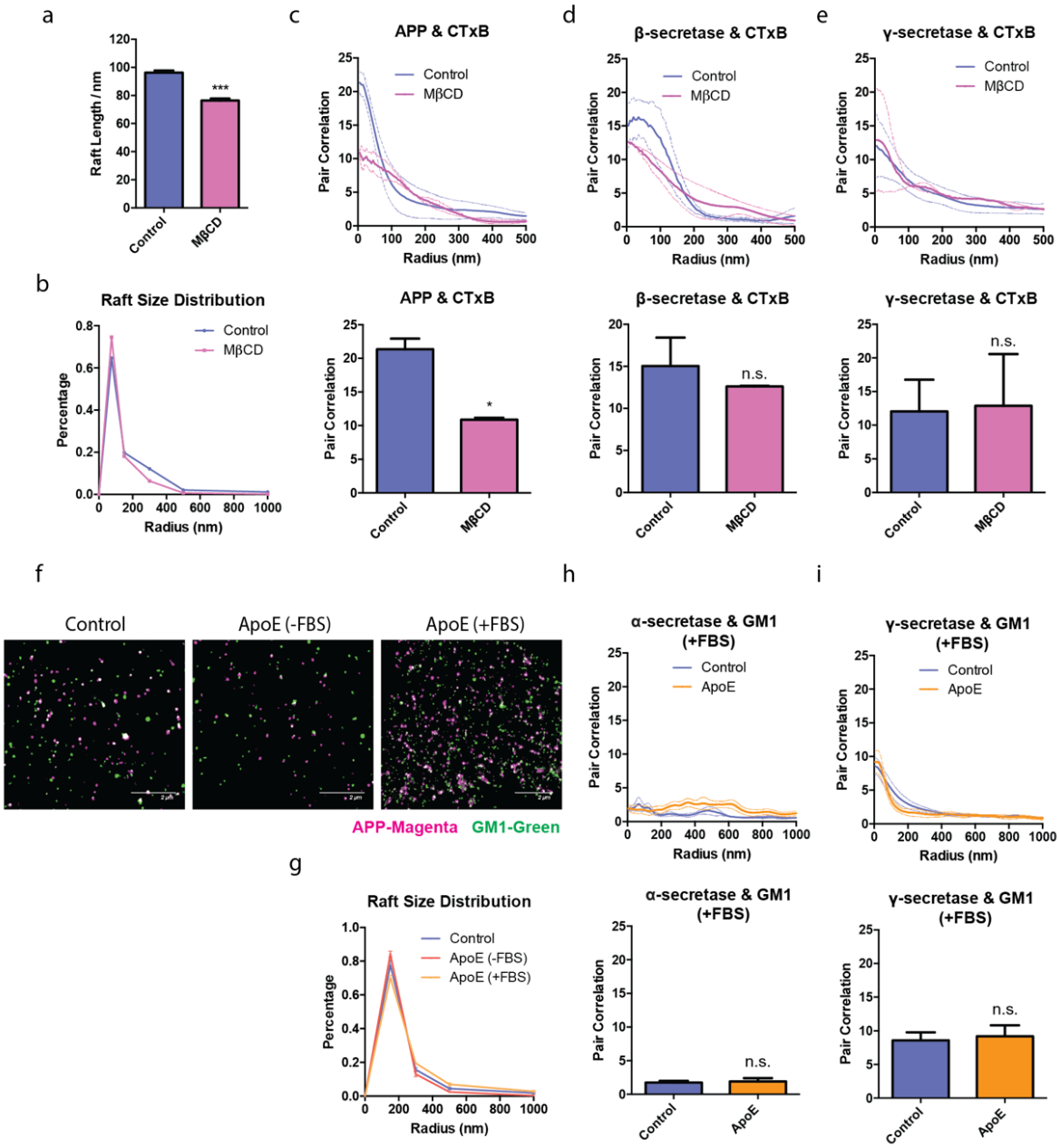

Figure S2. Super resolution imaging of enzymes and substrate localization with MβCD and apoE. (a) Apparent raft size of neuroblastoma 2a (N2a) cells before and after treatment with methyl-β-cyclodextrin (MβCD). (b) Cholesterol extraction by MβCD mediates a shift in raft size distribution from large rafts (>200 nm) to smaller rafts (<150 nm). (c) Lipid raft disruption by MβCD ejects APP out of lipid rafts into disordered regions. (d-e) β- and γ-secretase's lipid raft localization don't respond to MβCD-mediated raft disruption. (f) dSTORM imaging shows the effect of apoE on membrane protein's raft association (APP in magenta, GM1 in green) in N2a cells under low (no FBS) and high cholesterol (with FBS) conditions. Scale bar is 2 μm. (g) ApoE mediates a shift in distribution from small rafts (<150 nm) to larger rafts (>300 nm) under high cholesterol condition and opposite effect in low cholesterol condition. (h-i) α- and γ-secretase's lipid raft localization don't respond to apoE-mediated raft modulation under high cholesterol condition (with FBS). Data are expressed as mean ± s.e.m., n=3-10. *P<0.05, two-sided Student's t-test.

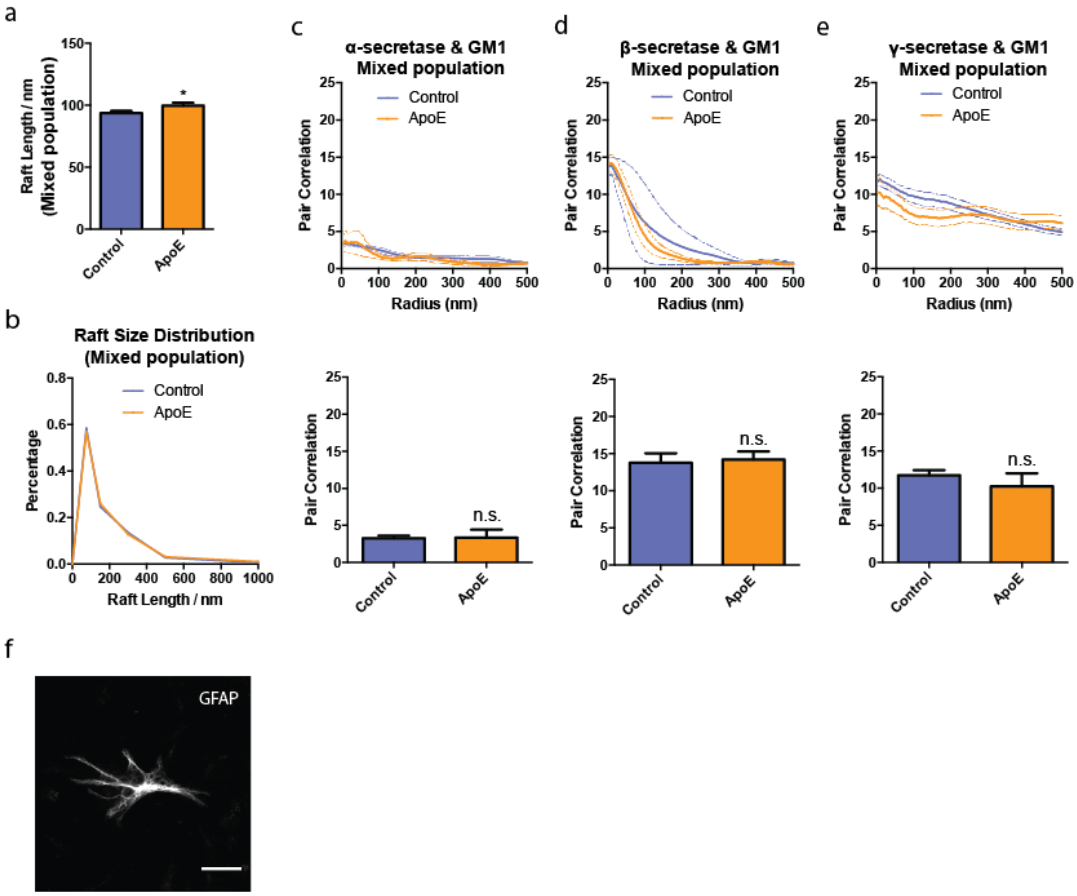

Figure S3. ApoE's effect on secretases in cortical neurons (a) Apparent raft size of primary cortical neurons before and after treatment with apoE in mixed culture with astrocytes. (b) Raft size distribution analysis showing apoE mediates a shift in distribution from small rafts (<150 nm) to larger rafts (>300 nm) in cortical neurons when culturing with astrocytes. (c-e) α-, β- and γ-secretase lipid raft localization in cortical neurons do not respond to apoE-mediated raft modulation when culturing with astrocytes. Data are expressed as mean ± s.e.m., n=3-10., two-sided Student's t-test. (f) Astrocytes in mixed cortical culture is labelled with GFAP antibody. Around 0.95% of the mixed cell population was GFAP positive.

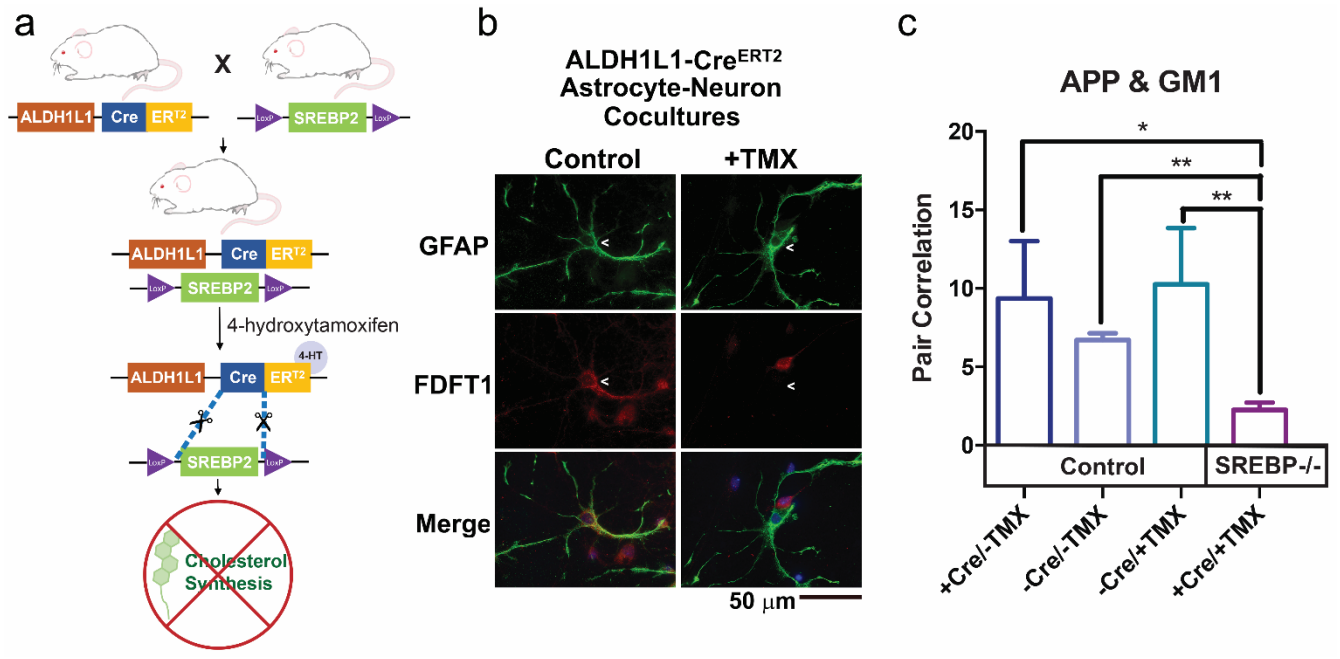

Figure S4. **Induction of astrocyte SREBP2 gene ablation disrupts the cholesterol synthesis enzyme FDFT1 and abolishes APP and GM1 pair correlation.** (a) Strategy for conditional knockout of SREBP2 in astrocytes using Cre-Lox recombination system. SREBP2 flox mice were crossed to ALDH1L1-specific Cre transgenic mice, which express Cre recombinase specifically in astrocytes when presented 4-hydroxytamoxifen (TMX). Cre promotes SREBP2 knockout and blocks cholesterol synthesis in astrocytes. (b) Astrocyte-neuron co-cultures are grown from ALD1L1-Cre^{ERT2} embryos. Astrocyte SREBP2 knockout is induced by application of 4-hydroxytamoxifen (TMX) to cultures. Following knockout, cells were immunostained for the cholesterol synthesis enzyme FDFT1 with the astrocyte marker GFAP and imaged. (c) Mixed primary cultures of neurons and astrocytes derived from SREBP2$^{flox/flox}$ x Aldh1L1-Cre and Cre negative littermates were treated with 4-hydroxytomoxifen (TMX) to delete SREBP2. APP lipid raft localization in cortical neurons is lost when SREBP2 is knocked out of astrocytes. TMX does not change APP localization in Cre negative cells.

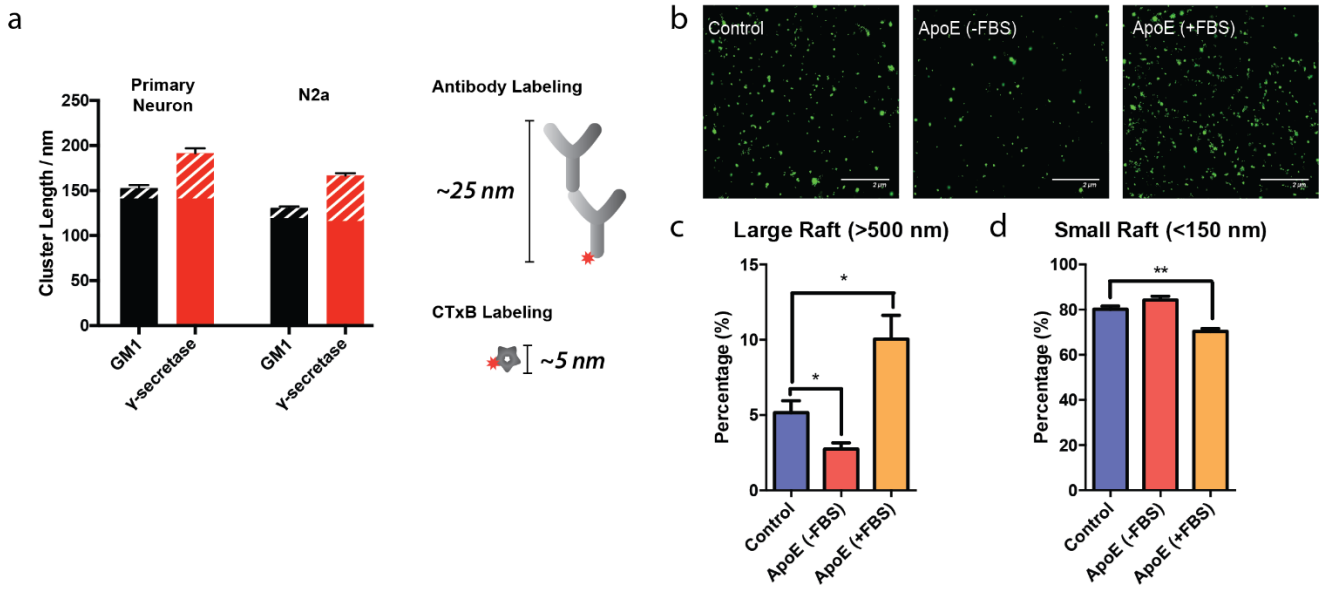

Figure S5. Analysis of raft size (a) Comparison of the size of CTxB labeled GM1 domains from primary neurons and N2a cells with antibody labeled γ-secretase. The potential added diameter from antibody or CTxB labeling is indicated by white stripes. Fixed γ-secretase within the GM1 lipids form clusters approximately the same size as CTxB labeled GM1 clusters, suggesting CTxB does not cluster unfixed GM1 lipids after treatment[73]. (b) dSTORM imaging shows the effect of apoE on GM1-labeled raft domains in N2a cells under low (no FBS) and high cholesterol (with FBS) conditions. Scale bar is 2 μm. (c-d) ApoE mediates a shift in distribution from small rafts (<150 nm) to larger rafts (>500 nm) under high cholesterol condition and opposite effect in low cholesterol condition. Data are expressed as mean ± s.e.m., *P<0.05, **P<0.01, one-way ANOVA.

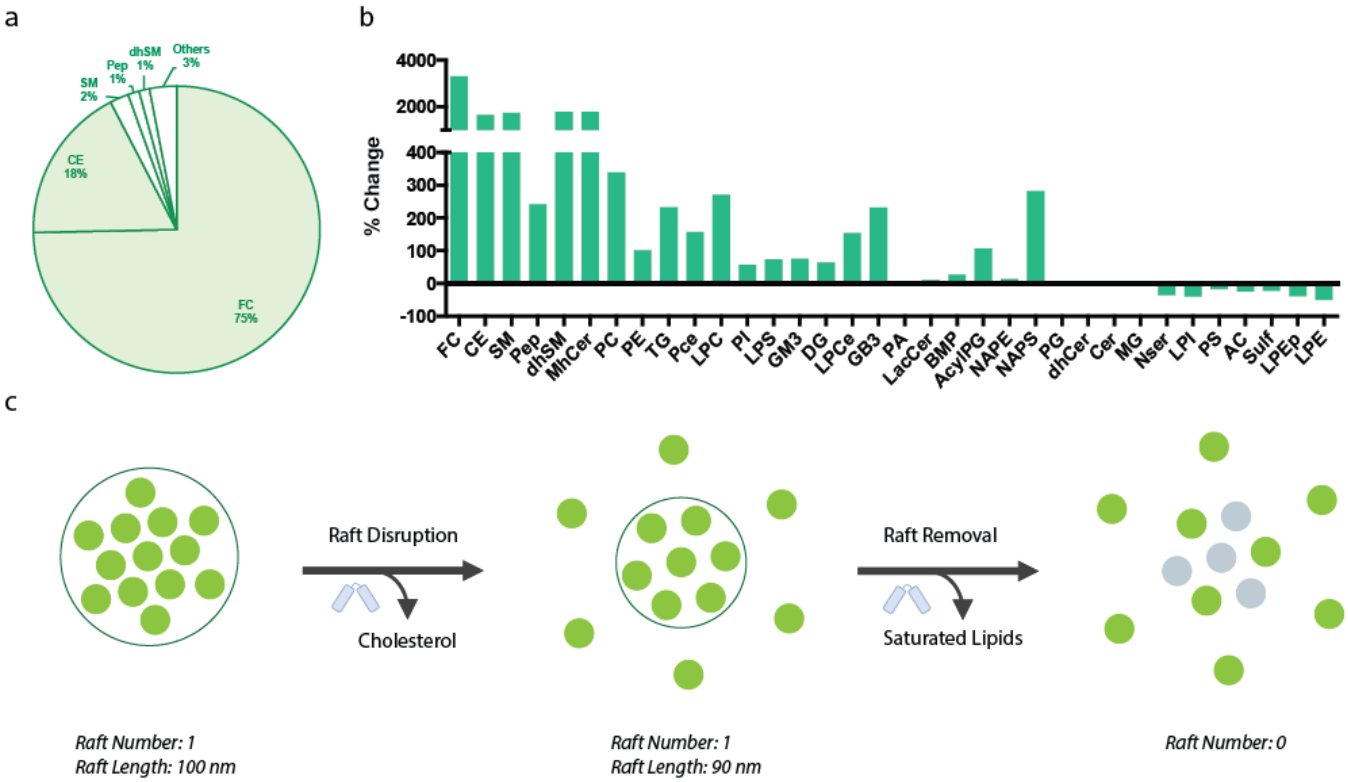

Figure S6. ApoE selectively extracts and transports raft lipids. (a) Lipidomics analysis showing 93% of lipids extracted by apoE from N2a cells are cholesterol. Some raft-associated lipids are also transported by apoE. (b) Relative changes in lipid concentration. %change = [c(after cell exposure) – c(before cell exposure)] / c(before cell exposure) x 100. (c) ApoE not only disrupts lipid rafts by cholesterol extraction, it can also remove lipid rafts bythrough extracting additional raft lipids. Abbreviations for lipids: FC, Free Cholesterol; CE, Cholesterol Ester; AC, Acyl Carnitine; MG, Monoacylglycerol; DG, Diacylglycerol; TG, Triacylglycerol; dhCer, Dihydroceramide; Cer, Ceramide; SM, Sphingomyelin; dhSM, Dihydrosphingomyelin; Sulf, Sulfatide; MHCer, Monohexosylceramide; GM3, Monosialodihexosylganglioside; PA, Phosphatidic acid; PC, Phosphatylcholine; PCe, Ether phosphatidylcholine; PE, Phosphatidylethanolamine; Pep,Plasmalogen phosphatidylethanolamine; PS, Phosphatidylserine; PI, Phosphatidylinositol; PG, Phosphatidylglycerol; BMP, Bis(monoacylglycero)phosphate; AcylPG, Acyl Phosphatidylglycerol; LPC, Lysophosphatidylcholine; LPCe, Ether lysophosphatidylcholine; LPEp, Plasmogen Lysophosphatidylethanolamine; LPI, Lysophosphatidylinositol; LPS, Lysophosphatidylserine; NSer, N-Acyl Serine.

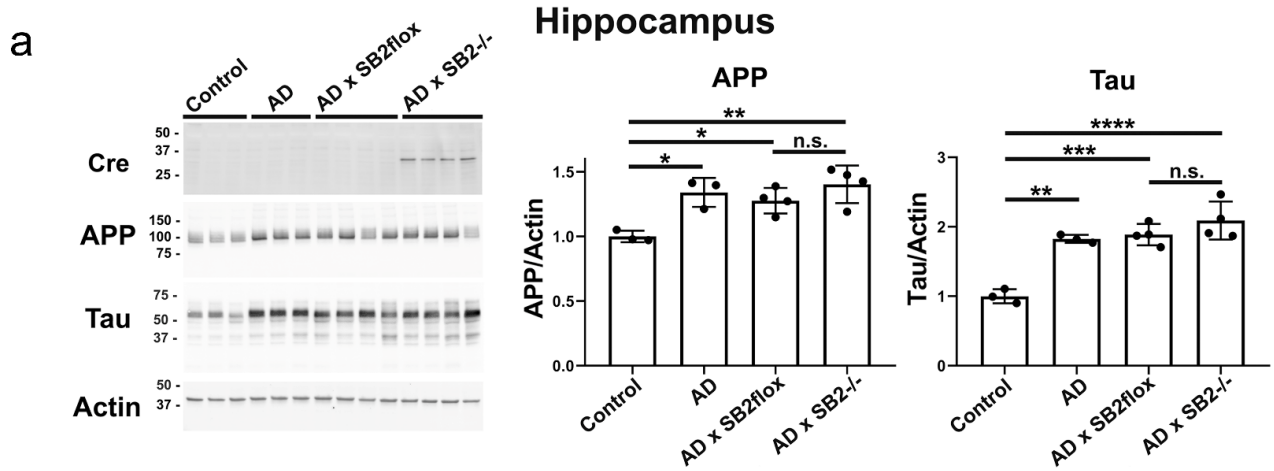

Figure S7. **Loss of astrocyte SREBP2 in the 3xTg AD models does not impact total transgene protein levels in the hippocampus.** 3xTg-AD (AD) mice express transgenes for mutant human amyloid precursor protein (APP) and Tau. The AD mice were crossed to SREBP2 floxed mice (AD x SB2flox) or to the SREBP2$^{flox/flox}$GFAP-Cre$^{+/-}$ mice (AD x SB2$^{-/-}$). Animals were aged 40 weeks and hippocampus tissue was dissected and homogenized for western blot. Data are expressed as mean ± s.e.m, n=3-4 animals per genotype. *P<0.05, **P<0.01, ***P<0.001, ****P<0.0001, one-way ANOVA with Tukey's post hoc analysis.